Development of a Roadside LiDAR-Based Situational Awareness System for Work Zone Safety: Proof-of-Concept Study
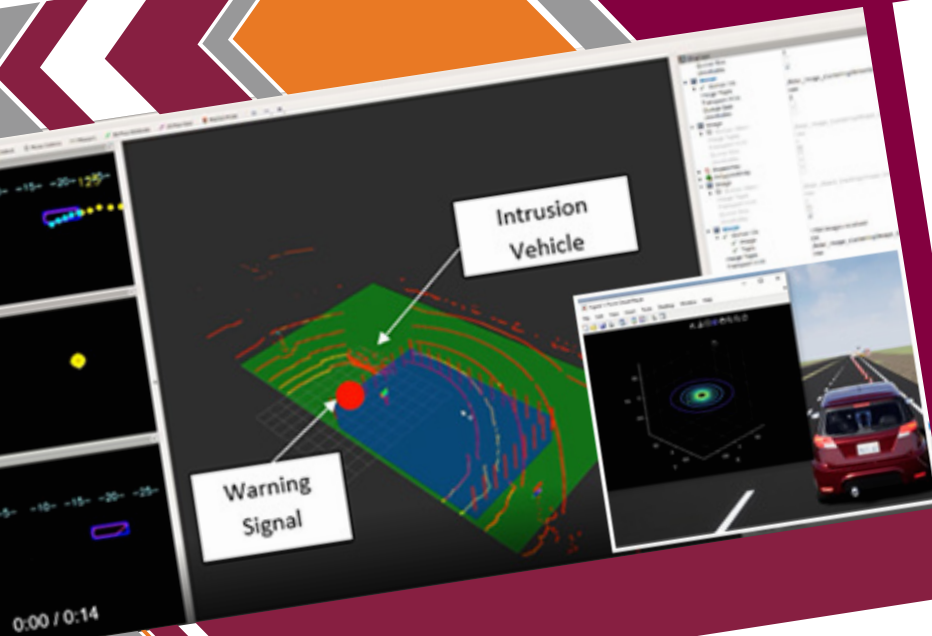
Intrusion Vehicle

Warning Signal

0:00 / 0:14

SAFE-D
SAFETY THROUGH DISRUPTION

VIRGINIA TECH
TRANSPORTATION INSTITUTE
VIRGINIA TECH.

Texas A&M Transportation Institute

SAN DIEGO STATE UNIVERSITY
Leadership Starts Here

Disclaimer

The contents of this report reflect the views of the authors, who are responsible for the facts and the accuracy of the information presented herein. This document is disseminated in the interest of information exchange. The report is funded, partially or entirely, by a grant from the U.S. Department of Transportation's University Transportation Centers Program. However, the U.S. Government assumes no liability for the contents or use thereof.

TECHNICAL REPORT DOCUMENTATION PAGE

1. Report No. TTI 05-03	2. Government Accession No.	3. Recipient's Catalog No.
4. Title and Subtitle Development of a Roadside LiDAR-Based Situational Awareness System for Work Zone Safety: Proof-of-Concept Study		5. Report Date September 2023
		6. Performing Organization Code:
7. Author(s) Jason (Dayong) Wu; Minh Le; Jerry Ullman; Tianchen Huang; Amir Darwesh; Srikanth Saripalli;		8. Performing Organization Report No.
9. Performing Organization Name and Address: Safe-D National UTC Texas A&M Transportation Institute 3135 TAMU College Station, Texas 77843-3135		10. Work Unit No.
		11. Contract or Grant No. 69A3551747115/[TTI 05-03]
12. Sponsoring Agency Name and Address Office of the Secretary of Transportation (OST) U.S. Department of Transportation (US DOT)		13. Type of Report and Period Final Research Report May 2020-September 2023
		14. Sponsoring Agency Code

15. Supplementary Notes
This project was funded by the Safety through Disruption (Safe-D) National University Transportation Center, a grant from the U.S. Department of Transportation – Office of the Assistant Secretary for Research and Technology, University Transportation Centers Program, and, in part, with general revenue funds from the State of Texas.

16. Abstract
Roadway construction and maintenance have become increasingly common as the U.S. transportation system ages and the population and traffic volume increase. This places more and more work zone workers near high-speed vehicles and increases the probability of being struck by them. This project innovatively deployed 360-degree LiDAR sensors at the roadside and tested their potential to provide work zone safety in terms of detection accuracy, efficiency, and ease of use. Researchers developed a set of algorithms to collect and interpret real-time information for each approaching vehicle and worker (e.g., location, speed, and direction) in and outside work zones using roadside LiDAR. Ultimately, the outcome of this pilot study could lead to developing a full-scale warning system deployable in a real work zone environment. Such a system could detect and analyze live traffic and work zone activity, activate the appropriate warning scheme, and deliver information to roadway workers in work zones in a timely manner so they can take evasive actions instead of relying on traditional "passive" safety countermeasures. This kind of panoramic, trajectory-level data for work zone actors can be used to develop a next-generation work zone situational awareness system.

17. Key Words LiDAR, Smart Work Zone, Safety, Situational Awareness System, Vehicle Detection/Tracking, Vulnerable Road User	18. Distribution Statement No restrictions. This document is available to the public through the Safe-D National UTC website, as well as the following repositories: VTechWorks, The National Transportation Library, The Transportation Library, Volpe National Transportation Systems Center, Federal Highway Administration Research Library, and the National Technical Reports Library.

19. Security Classif. (of this report) Unclassified	20. Security Classif. (of this page) Unclassified	21. No. of Pages 65	22. Price $0

Form DOT F 1700.7 (8-72)   Reproduction of completed page authorized

Abstract

Roadway construction and maintenance have become increasingly common as the U.S. transportation system ages and the population and traffic volume increase. This places more and more work zone workers near high-speed vehicles and increases the probability of being struck by them. This project innovatively deployed 360-degree LiDAR sensors at the roadside and tested their potential to provide work zone safety in terms of detection accuracy, efficiency, and ease of use. Researchers developed a set of algorithms to collect and interpret real-time information for each approaching vehicle and worker (e.g., location, speed, and direction) in and outside work zones using roadside LiDAR. Ultimately, the outcome of this pilot study could lead to developing a full-scale warning system deployable in a real work zone environment. Such a system could detect and analyze live traffic and work zone activity, activate the appropriate warning scheme, and deliver information to roadway workers in work zones in a timely manner so they can take evasive actions instead of relying on traditional "passive" safety countermeasures. This kind of panoramic, trajectory-level data for work zone actors can be used to develop a next-generation work zone situational awareness system.

Acknowledgements

Table of Contents

SAFE-D
SAFETY THROUGH DISRUPTION

SAN DIEGO STATE UNIVERSITY   Texas A&M Transportation Institute   VIRGINIA TECH TRANSPORTATION INSTITUTE

List of Figures

List of Tables

Introduction

Work Zone Safety

Roadway construction and maintenance have become increasingly common as the transportation system in the United States ages and the population and traffic volume increase. This fact places more and more work zone workers near high-speed vehicles and increases the probability of those workers being struck. According to the National Highway Traffic Safety Administration (NHTSA) and the National Work Zone Safety Information Clearinghouse, work zone crashes have consistently led to hundreds of fatalities and thousands of injuries each year (Figure 1). The economic and societal impact of these crashes is substantial, affecting not only those directly involved but also their families, communities, and the economy as a whole [1].
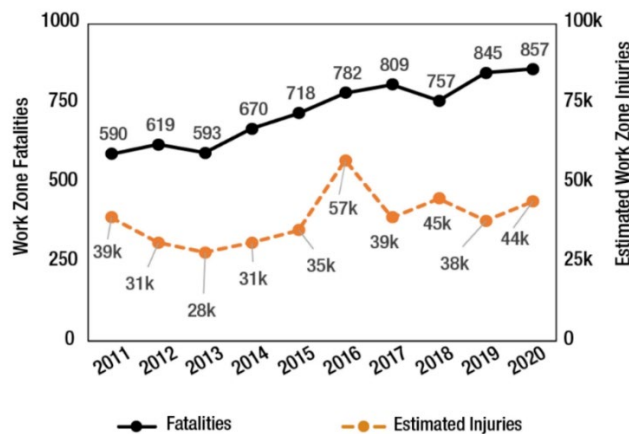
Figure 1. Graph. Fatalities and estimated injuries occurring in work zones, 2011 – 2020 [2].

Based on the New York State Department of Transportation Work Zone Accident Database, there were more than 3,400 traffic crashes and construction crashes over a 6-year period (2000-2005). Among them, 7.5% of all daytime crashes (133 in total) involved work zone intrusion, and 12.4% of nighttime work crashes (39 in total) involved an intrusion into the workspace. If focusing strictly on freeway lane closure work zones, the numbers are 9.7% and 14.2% for daytime and nighttime work zone crashes, respectively [3]. Another study from the Center for Construction Research and Training (CPWR) also indicated that the most common cause of road construction deaths between 2011 and 2016 was pedestrian vehicular incidents where a worker (nonoccupant of vehicle) was struck by a vehicle or mobile equipment (50.2%). Of the 267 pedestrian vehicular incidents, 61.4% were due to a worker (nonoccupant of vehicle) being struck by a forward-moving vehicle in the work zone (e.g., an intrusion vehicle from passing traffic),[1] followed by being struck by a vehicle backing up in the work zone (24.7%) [4]. Although only a small proportion of these intrusion

---

[1] It should be noted that the data does not differentiate between being struck by a motorist's vehicle going forward (i.e., a true intrusion) and a construction vehicle (dump truck or other vehicle) that was allowed in the workspace but that struck a worker on foot.

events involve a worker (approximately 8% to 30% depending on type of work zone and time of day) [3], construction workers are twice as likely to be killed by a motor vehicle than workers in any other industry sector [5]. Thus, improving work zone safety is one of the leading concerns for transportation agencies and highway contractors across the country.

Work Zone Safety Applications

Traditionally, efforts to reduce the risk of injuries and deaths have focused on improving work zone related traffic control devices, operations, and configurations to minimize collisions involving motorists. Such injury prevention measures include optimizing work zone layout, using temporary traffic control devices, motorist education and speed enforcement, high-visibility apparel, and work zone illumination [6]. However, inattentive or speeding drivers often disregard or ignore work zone traffic control devices and other warning information systems, which has led to work zone intrusions and serious crashes [7]. Because the work environment on the highway is often chaotic and noisy, it can be difficult for personnel to spot an errant vehicle in time to take appropriate action. Active strategies, such as deploying intrusion sensing and alerting technologies in highway work zones, may be an effective countermeasure in mitigating the risk of potential incidents in highway construction and maintenance sites.

Work Zone Intrusion Alert Systems (WZIAS) use sensing technologies and can help workers avoid an impending incident by detecting a vehicle intruding into the work zone and providing advance warning to the affected workers. Ideally, these systems would have alarm mechanisms that warn workers with enough time to properly react to the impending hazard [8]. The first such system was the product of a Strategic Highway Research Program (SHRP) sponsored study [9] and was introduced to work zones in 1995. Since SHRP, various departments of transportation (DOTs) have developed, evaluated, and implemented several other systems on their highway projects [7], [10]. These systems can be divided into three major categories:

- Mechanical systems use mechanisms, such as impact-activated or pressure-activated systems, that are triggered by physical contacts or impacts of intruding vehicles [11].
- Electronic systems apply sensing technologies such as ultra-wideband (UWB) [12], [13], Global Positioning Systems (GPS) [14], radio-frequency identification (RFID) [15], magnetic field [16], radar [17], infrared [18], laser [7], video [19], [20], and several others to detect intruding objects.
- Dedicated observers are workers or flaggers strategically positioned to spot intrusions and trigger alarms [19].

Although potential benefits were identified from these systems, only a few of them have been adopted by highway construction industry organizations. Some of the concerns reported about these technologies were effectiveness, cost implications of adopting new technology, and lack of technology feature synergy [7]. For example, the major limitation of mechanical systems is that the system's operator must be present at the time of a warning to notice any changes in work-zone barricade formations, while the major limitations of electronic systems are the frequency of false

alarms and the difficulty in setting up the systems. Table 1 summarizes these applications, with commercially available systems in bold. Developing innovative methods to reduce the number of crashes and vehicles intruding into the work zone is still critical.

Table 1. Existing WZIAS [7], [10]

Intrusion Technology Type	Intrusion System	States Tested	Commercially Available	Audible Alert	Visual Alert	Vibratory Alert
Mechanical	**SonoBlaster**	New Jersey DOT Kansas DOT	Yes	Yes	No	No
Infrared-Based	Safety Line	None	No	Yes	Yes	No
Pneumatic and Microwave	**Traffic Guard Worker Alert System**	None	Yes	Yes	Yes	Yes
Pneumatic and Microwave	**Intellistrobe**	Oregon DOT	Yes	Yes	No	No
Radar-Based	AWARE System	Missouri and Texas	No	Yes	Yes	Yes
Radio-Based	**Intellicone**	Kansas DOT	Yes	Yes	Yes	No
Radio-Based	Wireless Warning Shield	None	No	Yes	No	Yes
Laser-Based	ProAlert	None	No	Yes	Yes	No

LiDAR and Its Roadside Applications

Using advanced detection technology and edge processing to obtain reliable and enriched information about the various users in a multimodal traffic environment is the core function of intelligent transportation systems (ITS). The current ITS sensors such as loop detectors, video cameras, microwave radars, and Bluetooth sensors mainly provide macro traffic data, namely traffic flow rates, average speeds, and occupancy. However, new traffic systems and applications such as connected and autonomous vehicles (CAVs), adaptive traffic signal control, near-crash analysis, and automatic pedestrian crossing warning system require traffic flow information with more detail and higher accuracy—especially high-accuracy, high-resolution trajectory data for all users in a multimodal traffic environment.

As a type of active vision sensor, a light detection and ranging (LiDAR) sensor emits pulsed light waves into the surrounding environment. These pulses bounce off surrounding objects and return to the sensor. The sensor uses the time it took for each pulse to return to the sensor to calculate the distance it traveled. Repeating this process millions of times per second creates a precise, real-time 3D map of the environment. This 3D map is called a point cloud. LiDAR shows its great potential

in providing high-resolution micro traffic data (HRMTD) through a 360-degree detection of the surrounding environment in real time (Figure 2). It also has advantages of insensitivity to external light changes, strong adaptability to complex environments, high accuracy and frequency, wide coverage, and enriched depth information [21]. Especially when deployed at the infrastructure level, LiDAR can obtain the high-resolution fine-grained position, direction, speed, and even the trajectory of each road user within the scanning range, which could be used as a valuable data input for vehicle-to-everything (V2X) and Cooperative Vehicle Infrastructure System (CVIS) applications (Figure 3 shows some examples).

(a) (b)
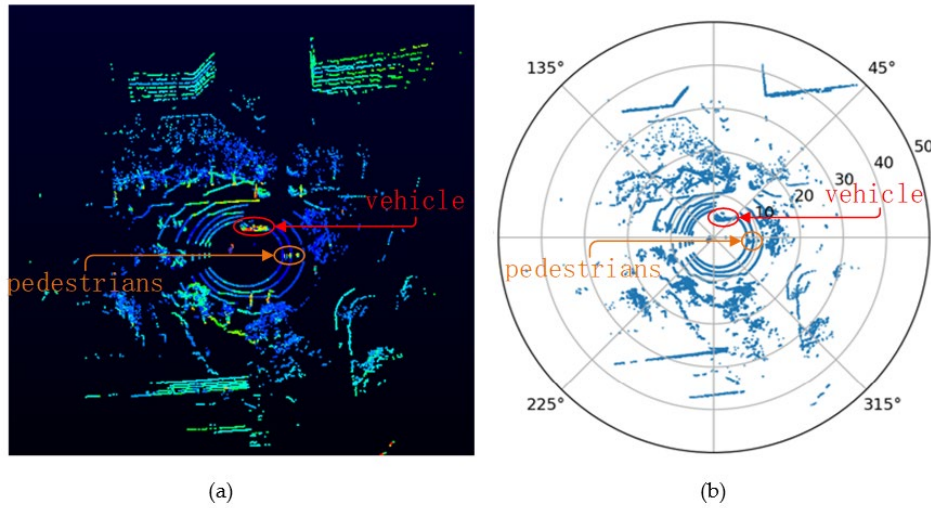
Figure 2. Images. A LiDAR 3D point cloud data:

(a) Original point clouds displayed in the VeloView™ software; (b) The projected point cloud in the polar coordinate system.

Figure 3. Photos and text. Current roadside or infrastructure-based LiDAR ITS applications in Nevada and Tennessee [22].

Currently, the most typical LiDAR application is to detect roadway and traffic information for automated driving vehicles [23]. However, a growing number of roadside LiDAR applications and studies can be found in the field [24], [25], though most are still in the proof-of-concept stage [26], exploring this possibility [27], [28], or just providing some system prototypes [29].

The HRMTD for all work zone "actors" (e.g., workers, construction equipment, passing vehicles) can be collected simultaneously and in real time by a LiDAR sensor, including each work zone user classification, presence, location, speed, and direction. This kind of panoramic, trajectory-level data of work zone actors can potentially be used to develop an intelligent and reliable work zone situational awareness or intrusion alert system. In other words, LiDAR can be a potentially powerful sensing technology to significantly improve intrusion sensing accuracy and speed while reducing false alarms.

Motivations of this Study

This project innovatively deployed 360-degree LiDAR sensors at the roadside and tested their potential for providing work zone safety in terms of detection accuracy, efficiency, and ease of use. The objective of this pilot study was to develop a set of algorithms to collect and interpret real-time information of each approaching vehicle and worker (e.g., location, speed, and direction) in and outside work zones using the roadside LiDAR sensing equipment. Ultimately, the outcome of this pilot study could lead to the development of a full-scale warning system that is deployable in a real work zone environment. Such a system could detect and analyze live traffic and work zone activity, activate the appropriate warning scheme, and deliver information to roadway workers in work zones in a timely manner so that they can take evasive actions instead of relying on traditional "passive" safety countermeasures. This kind of panoramic, trajectory-level data of work zone actors can potentially be used to develop an intelligent and reliable work zone situational awareness or intrusion alert system.

This research addressed the following research questions:

1) Can we use the emerging 360-degreee roadside LiDAR sensing technology to provide advance warning of potential vehicle intrusions? What are potential barriers for a LiDAR-based intrusion alert system?
2) How can we develop a set of algorithms to detect, classify, and track vehicles and "pedestrian" workers with high accuracy and in real time? Is a LiDAR-based intrusion alert system more reliable than other systems (e.g., avoiding false alarms)?
3) What work zone scenario(s) has/have the most need to be tested for preventing potential vehicle intrusions (e.g., two-lane highway with low-medium speed, four-lane freeway with high speeds)?
4) How can we properly test and validate the algorithms in designed experimental scenarios in terms of reliability, accuracy, and computational efficiency?

5) How can we provide proof of concept for such a work zone awareness system in a real work zone environment? What is the optimal detection setup (single vs. multiple sensors, location, height, etc.) given specific work zone configurations?

Data Collection and LiDAR Datasets

In this section, the datasets utilized in the research project to develop and evaluate a LiDAR-based work zone intrusion system will be discussed (Figure 4). By utilizing a variety of datasets, including simulated data, data from test sites, data from a controlled work zone experimental site, and data from real work zone sites, researchers thoroughly evaluated and refined the LiDAR-based work zone intrusion system. The details of each dataset, data collection methodologies, and insights gained can be found in Appendix B, providing a comprehensive understanding of our system's development and performance.
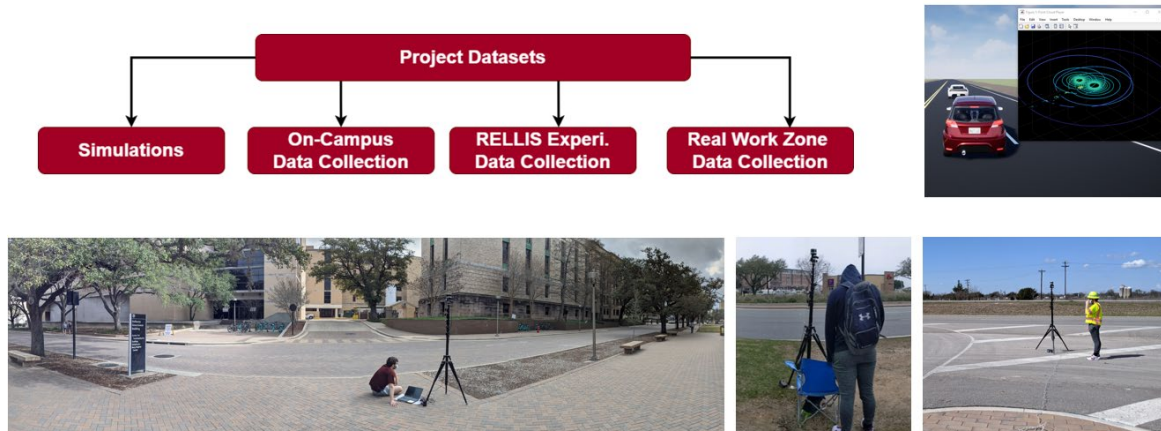
Figure 4. Photos and diagram. Data collection and LiDAR datasets used in this study.

System Development

In this innovative project, 360-degree LiDAR sensors were strategically installed at the roadside to evaluate their effectiveness in enhancing work zone safety. The primary focus was on assessing the detection accuracy, efficiency, and user-friendliness of these sensors. The pilot study aimed to develop algorithms capable of capturing and analyzing real-time data about vehicles and workers, including their location, speed, and direction, both within and outside the work zones. The roadside LiDAR sensing equipment played a crucial role in achieving this objective, enabling the collection and interpretation of valuable information to improve overall work zone safety measures. At a high level, the developed system included or consisted of the following functions:

- Detect 2D (x, y) position of vehicles in the adjacent lanes of the work zone.
- Perform data association and tracking of detected vehicles (for inflow and outflow monitoring and position filtering).
- Assess tracked vehicles' behaviors to accurately determine threats.

- Accurately determine or predict threats.
- Send an intrusion alert.

The system has the following modules (Figure 5 and Figure 6):

1) Point Cloud to Image Module
2) Image Module to Clusters Module
3) Clusters Module to Detection/Tracking Module
4) Trajectory Extraction Module
5) Intrusion Risk Prediction/Warning Module
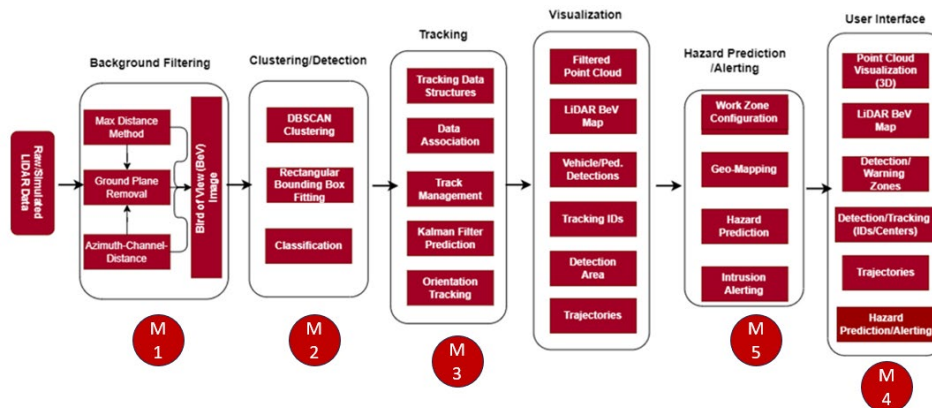
Figure 5. Flowchart. The developed system and its modules.
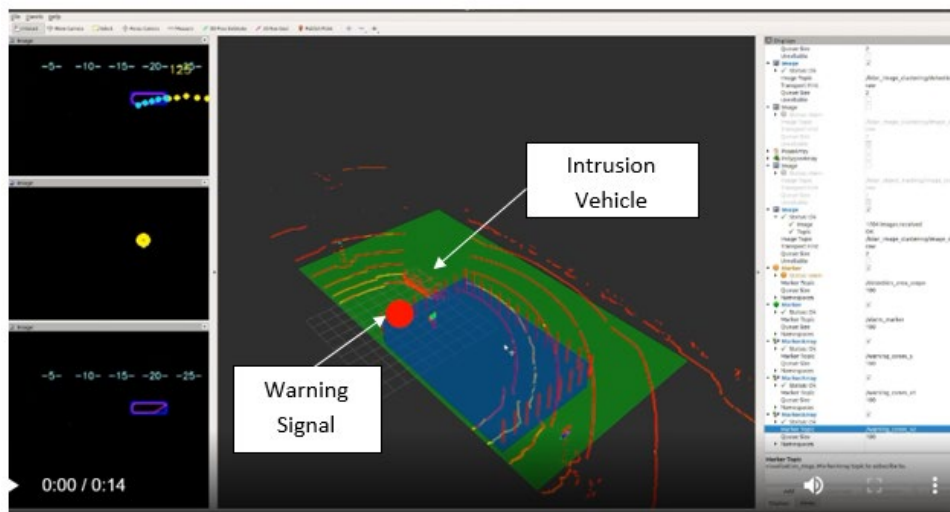
Figure 6. Screen shot. Visualization of the system interface.

System Configuration and Calibration

The success of any LiDAR-based application, especially one focused on detecting work zone intrusions, heavily relies on the proper configuration and calibration of the LiDAR system. In this

section, we will delve into the details of the system components, their arrangement, and the calibration procedures employed to achieve accurate and reliable detection results.

The LiDAR system utilized in this work zone intrusion detection application is the Ouster OS-1 32 LiDAR. The LiDAR operates at a wavelength of 1,550 nm and is equipped with a rotating mirror mechanism to capture a 360-degree view. The system we developed processes the LiDAR point cloud data in real time. The LiDAR sensor is strategically mounted on a sturdy tripod approximately 1.5 to 2 m above ground level at the roadside, facing the work zone. The sensor's mounting position is selected for an unobstructed 360-degree view of the surroundings, including the work zone and potential intrusion paths. Careful consideration is given to avoiding occlusions from nearby objects like signposts or vegetation that might hinder the sensor's line of sight.

The LiDAR system's data is recorded in a local Cartesian coordinate system, with the LiDAR sensor as the origin. To georeference the LiDAR measurements to real-world coordinates, a Global Navigation Satellite System (GNSS) receiver is co-located with the LiDAR sensor to obtain accurate positional information. The GNSS data is post-processed and fused with the LiDAR data using a Kalman filter to compute precise georeferenced point cloud data. In this project, we only tested the georeferencing process in experiments on the Texas A&M University (TAMU) RELLIS Campus.

Perception Requirements

Different sensors provide varying levels of fidelity, each with their drawbacks. Commercially available traffic monitoring radar systems, including direct and side-fired radars, have been used to detect and track vehicles up to 300 m [30]. Radar measurements, however, are lower in fidelity, detecting only the vehicle pose/velocity, and can often be noisy, which decreases accuracy [31].

Optical machine vision sensors have also been used in traffic detection for both pose and orientation [31], though they can suffer from poor accuracy in nighttime operation. Although the percentage of work zone nighttime crashes is lower than in daytime traffic (due to higher volumes), crash rates per million vehicles are substantially higher at night [32], [3]. Cameras also require extrinsic/intrinsic calibration, which relates the image pixels to a physical point in 3D space. A work zone is a dynamic site; researchers determined that the sole use of cameras was not feasible due to lengthy setup times with calibration, especially if this process must be repeated multiple times. Day/night operation requirements also warranted a different or additional sensing modality.

3D LiDAR offers a higher resolution than radar, which not only allows increased accuracy in position estimation but can also allow detection of the orientation of the vehicle. LiDAR is also not subject to varying lighting conditions and produces a 3D point cloud rather than 2D pixel images. Calibration is more straightforward, as the operator would only need to provide semantic information such as the road and work zone area in a 3D map. As LiDAR technology progresses with reduced costs, we still forecast its use as a vital component in developing a Smart Work Zone (SWZ). These can include systems with multiple LiDARs and in combination with other sensors.

[2]The team started by researching the theoretical capabilities—which vary based on the LiDAR model, configuration, and resolution—to issue guidance on the LiDAR model and placement for roadside application. For these purposes, a highway posted at 65 mph (104 kph) was defined as having four travel lanes 3.6 m wide in each direction. In one direction, the far right lane is closed as part of the work zone, including the 2.4 m wide shoulder.

Let the horizontal placement D_h be the distance between the LiDAR and edge of the closest open lane and D_v be the vertical mounting distance from the ground (Figure 9). Setback distances are limited to the work zone (i.e., $0 \leq D_h < 6.0$ m). The placements D_h, D_v, horizontal and angular resolution γ, φ, and number of LiDAR beams n_{beams} dictate the spacing between the returned points. As the spacing increases with the beam distance, the vehicle detection range diminishes.

To define the spacing between points, consider two simplified concepts on one side of an eight-lane highway. In the first scenario, only consider the horizontal spacing A_k distances in the XY plane for LiDAR measurements taken against an imaginary flat wall, visualized in Figure 8, with A_k given by Equation (1). Extending the imaginary wall to a vehicle, A_k represents the separation distance between points taken on the side from bumper to bumper. In another scenario, the horizontal B_k and vertical C_k spacing distances are considered for measurements in the XZ plane, visualized in Figure 9 and given by Equation (2) through Equation (4). These represent the spacings from the tires to roof (C_k) and the distances between points on the roof (B_k). A conically shaped blind spot lies directly underneath the LiDAR that varies in angle and radius based on the placement. This is characterized by the minimum height $\delta_{\min}$, and an object is detectable at distance D_h.

$$A_n = D_h(\tan n\phi - \tan(\phi(n-1))) \qquad (1)$$
$$C_k = D_h(\tan k\gamma - \tan(\gamma(k-1))) \qquad (2)$$
$$\delta_{\min} = D_v - D_h \tan K\gamma \qquad (3)$$
$$B_k = \frac{D_v - \delta_{\min}}{\tan k\gamma - \tan(\gamma(k-1))} \qquad (4)$$

There are several competing metrics affected by adjusting the LiDAR placement[2]. The first priority is to ensure that $\delta_{\min}$ remains low enough that at least a portion of the vehicle side is detectable. It is also desirable to keep C_k sufficiently small to observe multiple beams on a vehicle. If there is enough resolution, we can design for a $\delta_{\min}$ that allows us to cover side and vehicle roof.

The theoretical spacing results for both the popular VLP-16 and the less common Ouster OS1-32 are shown in Figure 7. Note that only half the VLP-16's beams are utilized for vehicles shorter than D_v. The OS1-32 not only has more than twice as many beams, but it can also be manufactured

---

[2] A control parameter of interest is not studied, β, the pitch relative to the ground. Adjusting the pitch will unilaterally increase the utilized in beams in one side. In on-going work we are considering worker detection, which may not be possible with certain pitches. Further, in specially designed LiDARs, the pitch may not need to be adjusted.

to vertically scan below zero (down to −22.5°). This allows the full utilization of the 32 beams and concentrates on the γ resolution.

For the spacing analysis, researchers fixed the vertical mounting distance at 2.2 m, as this allowed the flexibility to detect both the roofs and the sides of most vehicles. Observing the A_k spacing results, the limitations on tracking ranges are quickly evident. Beyond $A_k > 0.5$, too few points are received to reliably detect a vehicle. Results for B_k demonstrate that the VLP-16 cannot observe multiple bands of points of the roofs and that the vehicle sides are mostly detected via C_k. Though it is possible for vehicles in all lanes to be detected, severe occlusions will occur when the closest lane is occupied. However, there are better results for B_k, and the roofs of the vehicles in the closest lane can likely be detected with the full utilization of the OS1-32. Researchers did not have a below-horizon configured OS1-32 for testing, but we hypothesize that the tracking distances should improve ±20 to 25 m, or 45 m in total, based on the spacing distances A_k. Hence, considerations of the placement and LiDAR configuration as it relates to the application will allow for greater utilization of the sensor. Selecting a sensor configured to scan below the horizon such as the OS1-32 with resolutions $\varphi = 0.17°$ and $\gamma = 0.70°$ and placement at $D_h = 4 − 6$, $D_v = 2.2$ m would allow detection of both vehicle sides and roofs for up to one to two lanes, as seen in Figure 7.

(a) Velodyne VLP-16, $D_v = 2.2m$ $\omega = 10Hz$ (b) OS1-32, $D_v = 2.2m$ $\omega = 10Hz$
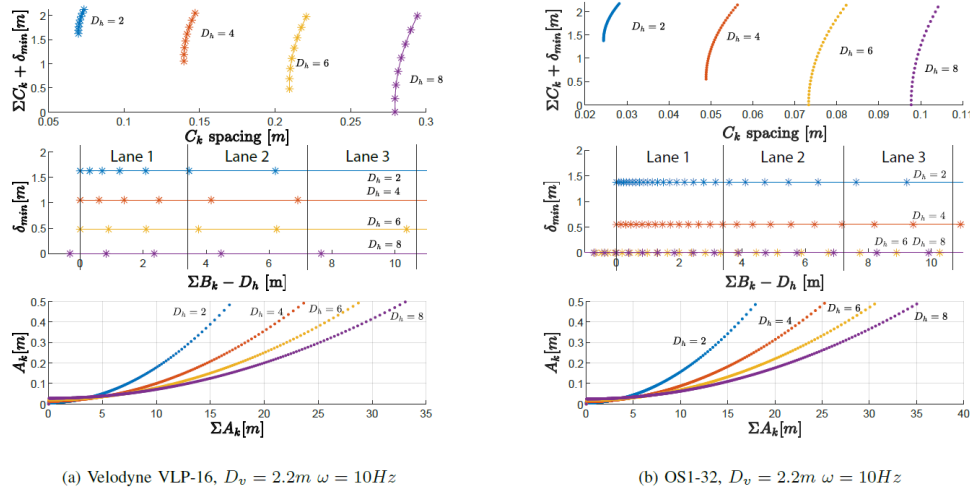
Figure 7. Graphs. A_k, B_k, and C_k theoretical spacing results. $\Sigma C_k + \delta_{min}$ represents the distance from the ground, $\Sigma B_k − D_h$ represents the horizontal spacing along the lanes, while ΣA_k is the longitudinal spacing along the lane [33].
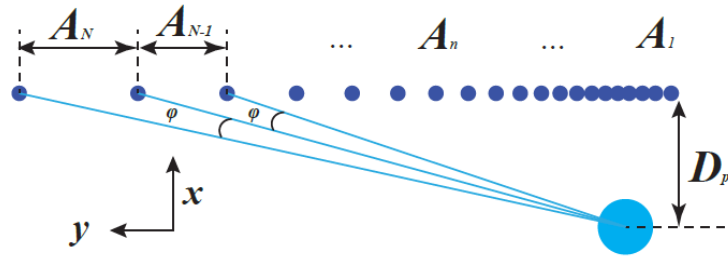
Figure 8. Graph. Horizontal spacing in XY plane between points for a 2D scan of a flat wall with the LiDAR sensor positioned D_h away. n ranges from $N = 1$ to $N = \pi/\varphi$ [33].
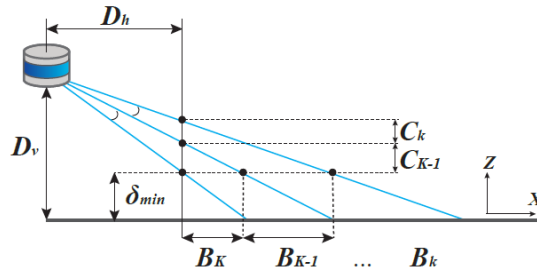
Figure 9. Graph. Horizontal/vertical spacing between points in the ZX plane at _min. The mounting height D_v and setback distance D_h from the road affect the spacing [33].

Communication and Alarm Considerations

Researchers also considered the alarm as it relates to sensor update rates, worker notification, and processing requirements. The sensor update rate ranges are given by the LiDAR manufacturer—the VLP-16 is configurable from 5 to 20 Hz, while the Ouster OS1 series can either be 10 or 20 Hz. Because the total number of points per second remains the same, the horizontal resolution changes depending on the rotation rate ω. An appropriate ω must balance the horizontal resolution φ, while also providing a fast enough update rate to accurately predict threats. At 104 kph (65 mph) and $\omega = 10$ Hz, the position difference between updates is 3 m. Doubling ω reduces the position difference by half, but the resolution φ doubles to 0.4° with the VLP-16. Determining the minimum frequency ω required to accurately predict threats is still under active study, but researchers selected $\omega = 10$ Hz for the current methodology to balance resolution and the update rate.
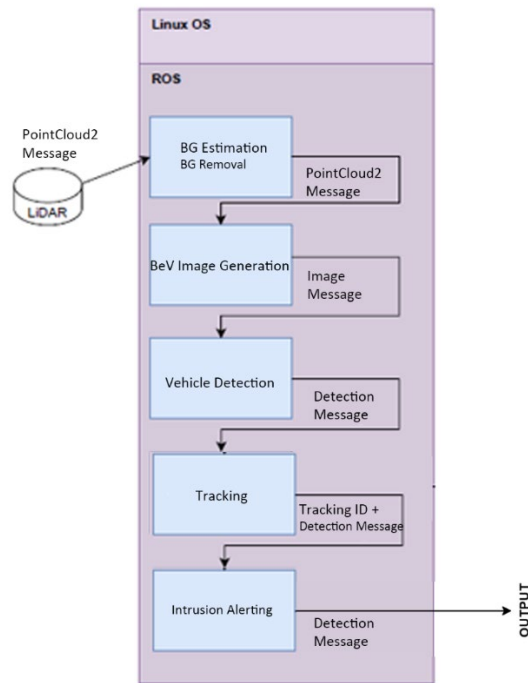
Figure 10. Flowchart of the developed system architecture.

For processing requirements, the detection algorithms should run at an update rate at least as fast as the sensor frequency. Because the processing happens onsite in real time for threat prediction, it is highly desirable to produce lightweight algorithms.

Methodology

Platform and Software
For this work, researchers designed the system architecture using the popular Robotic Operating System (ROS) [34] as the middle-ware software. Each system sub-task is designed in components to run separately on "ROS-nodes," as illustrated in Figure 10. The algorithms for this research were developed in C++ and Python utilizing the open-source Point Cloud Library (PCL) [35] and OpenCV Libraries [36]. With ROS's portability and standardized messages, researchers were able to deploy on multiple types of machines and even use different types of LiDAR sensors.

Background Removal
Background removal is the process in which stationary objects, such as the ground readings, are removed from the point cloud. In the case where the LiDAR is static, the background removal process is much simpler than the dynamic case. Researchers applied a common methodology using the "Max Distance" [37] or "Azimuth-Channel-Distance" [38] method. In this procedure, the background is subtracted based on maximally recorded distances for each beam of the LiDAR, which assumes the background is impenetrable.

Figure 11 illustrates a scenario of readings of two beams at $t_{0;1}$. Because the true background point $P_{i,j}|t_1$ exists outside the region of interest (ROI), $P_{i,j}|t_0|_2$ is incorrectly chosen as the maximum background distance. Therefore, it is desired to (1) collect the distances when no or few vehicles are present, and (2) set the distance to 1 for any beams not measured during this time. However, solving (1) requires manual operation to start the background collection when no vehicles are present. To solve this issue, an initial background estimate can be measured for a tunable number of frames, which removes the majority of the background (but also includes some false positives). Subsequently, the vehicle detection algorithm can be started, and when there are a few numbers of detected vehicles, the background can be recomputed online. Further robustness may be added in cases where the background changes over time.
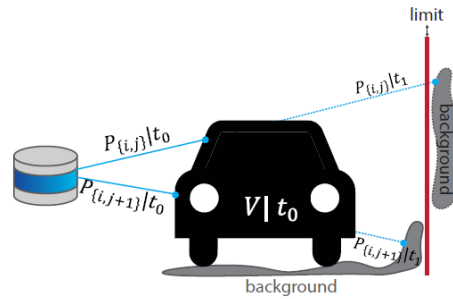
Figure 11. Diagram. LiDAR readings for $t = 0, 1$. At t_0, the vehicle occludes beams $P_{i,j}$, $P_{i,j+1}$ path. At t_1, the vehicle is gone, and the previous beams fall incident on the world background [33].

Bird's-eye View Image Generation

Vehicles in LiDAR data are easily distinguishable by a bird's-eye view (BeV). This 2D projection of the LiDAR data provides a simple and efficient way to cluster vehicles. A binary or RGB color image can be used, depending on what features are to be encoded. In this methodology, researchers utilized a binary image $I(x, y)$ defined by:

$$I(px, py)^{m \times n} \in \{0, 1\}$$
$$\text{where:}$$
$$px = int_{16}((x + |x_{min}) * scale + 0.5)$$
$$py = int_{16}((y + y_{min}) * scale + 0.5)$$

(5)

Hence, even with multiple point pairs (x, y) at different heights z, the bitmap will remain 1. In other methodologies, the height and intensity values can be encoded by using multiple color channels, which has been useful in deep learning-based approaches [39].

It is recommended that a limit $x_{min} \leq x \leq x_{max}$, $y_{min} \leq y \leq y_{max}$ be applied to bound and pre-allocate the image dimensions $m \times n$. The image scale can be empirically chosen; in these experiments, researchers found that a scale of 8 to 10 worked best for a 15×60 m area. The scaling factor affects the precision of the data—a scale factor of 10 pixels per meter will have a precision of ± 10 cm. Computing BeV images spent less than 1 millisecond (ms) of computation time.

Vehicle Detection

1) Clustering: After the BeV image is generated, a clustering scan algorithm can be used to generate potential image detections. Density-Based Spatial Clustering of Applications with Noise (DBSCAN) has been a popular method for clustering LiDAR data [38], [40]. Two parameters, ε and η_{min}, are utilized; however, the LiDAR's characteristic of returning sparse point clouds as the radial distances increases makes it difficult to choose a single ε value. Zhao proposed a variable ε based on the radial distance from the LiDAR [38]. Researchers applied a dilation operation w_k to the BeV image η_d times prior to clustering, which increases the density of partial vehicle scans. Experimentally, we found that a single operation of a 3×3 dilation kernel of ones is sufficient for clustering with $\varepsilon = 8$, $\eta_{min} = 15$.

2) Vehicle Detection: After the clusters have been generated, classification is needed to determine if the track is a vehicle. Common methodology for classification includes Support Vector Machines (SVM). In [41], a 28-feature SVM for vehicle classification in mixed urban environments was utilized. The current study is primarily interested in detecting vehicles, so researchers simply categorized between vehicle and nonvehicle based on the area, dimensions, and dimension ratio of the detection. Examples of nonvehicle detections can include pedestrians, noise, and small partial scans of vehicles. Lastly, the cluster bounds in the dilated image are then used to find the bounding box in the original image. A pseudocode of the vehicle detection process is shown (Algorithm 1) is shown in Figure 12. The overall detection process is illustrated in Figure 13.

Algorithm 1: Vehicle Detection

Input: Dilation Kernel w_k, convolution ops η_d
Data: BeV LIDAR bitmap $f(x,y)^{m \times n} \in \{0,1\}$
Output: Detections: [Pos. c_x, c_y, Dimensions w, h]
$P \in \mathbb{R}^{mn \times 2} \leftarrow \texttt{ImgToPts}(f(x,y))$
for $i \leftarrow 1$ **to** η_d **do**
  $\quad f(x,y) \leftarrow w_k * f(x,y);$
end
$P_g \in \mathbb{R}^{mn \times 2} \leftarrow \texttt{ImgToPts}(f(x,y))$
$b_{boxes}, clusters \leftarrow \texttt{DBSCAN}(P_g, \epsilon, n_{min})$
for $i \leftarrow 1$ **to** $len(clusters)$ **do**
  $\quad$ **if** $\texttt{Classify}(clusters[i])$ **is vehicle then**
    $\quad\quad$ // use undilated points
    $\quad\quad b_{boxes}[i] \leftarrow \texttt{RefineBbox}(b_{boxes}[i], P)$
  $\quad$ **else**
    $\quad\quad b_{boxes}[i].\texttt{del}()$
  $\quad$ **end**
end

Figure 12. Text image. Vehicle detection algorithm [33].
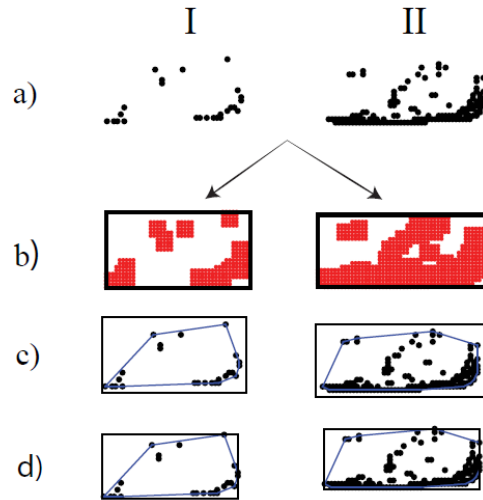
Figure 13. Graphs. Image dilation and detection process for two different vehicles (I-II). (a) BeV points, (b) points after dilation and corresponding cluster bounding boxes, (c) cluster search on original points, and convex hull generation, and (d) refined cluster bounding boxes [33].

Vehicle Tracking

Multi-object tracking (MOT) involves four consecutive stages: (1) object detection, (2) data-association, (3) prediction, and (4) track life-cycle management. Several methods have been developed for data association depending on the context and application. Some methods include the Joint Probabilistic Data Association Filter (JPDAF) [42] and the Hungarian/Munkres algorithm [43]. As a starting point, the team used the Hungarian algorithm due to its simplicity. The cost function is based on the Euclidean separation distance between new detections and predicted vehicle positions. The detections are assigned to tracks based on the lowest cost, though they must be within a maximum distance cost $\Delta_{\text{max-cost}}$. A life-cycle observer removes tracks that have had more than $\eta_{invisible}$ frames and tracks whose center position has transitioned near the end of the ROI. Unassigned detections typically (though not exclusively) result from the following: (1) a new vehicle that is untracked, (2) multiple partial detections for a new or already tracked vehicle, and (3) detections from a previously deleted tracked vehicle(s). Lastly, for prediction and filtering, the team used a discrete constant velocity Kalman filter running at the same frequency as the LiDAR setting. The tracking execution time did not exceed 3 ms.

Vehicle Trajectory Extraction and Prediction

The Kalman filter is a mathematical algorithm used to estimate the state of a system based on a series of noisy measurements. It was first developed by Rudolf E. Kalman in 1960 and has since become a widely used technique in many applications, including vehicle trajectory tracking and predicting. An overview of the Kalman filter, its formula, its applications in vehicle trajectory tracking and predicting, and its advantages appear in Appendix A.

Researchers used the Kalman filter to track and predict the trajectory of detected objects [44]. The Kalman filter can offer estimates for certain unknown variables observed over time via given measurements. Upon initialization, the Kalman filter anticipates the system state for the

subsequent step while also giving the prediction's uncertainty. After a measurement has been taken, the Kalman filter revises (or adjusts) the prediction and the present state's uncertainty. Simultaneously, it predicts future states in a continuous manner.

Vehicle Intrusion Alerting

Figure 14 shows the threat alert system. First, researchers set a buffer called the warning zone; the distance of the warning zone to the edge of the detection zone is D, and the distance between the vehicle and the detection zone is d. When a vehicle approaches the detection zone, if it reaches the warning zone ($d <= D$), it would be considered a threat. At this point, a warning signal is sent.
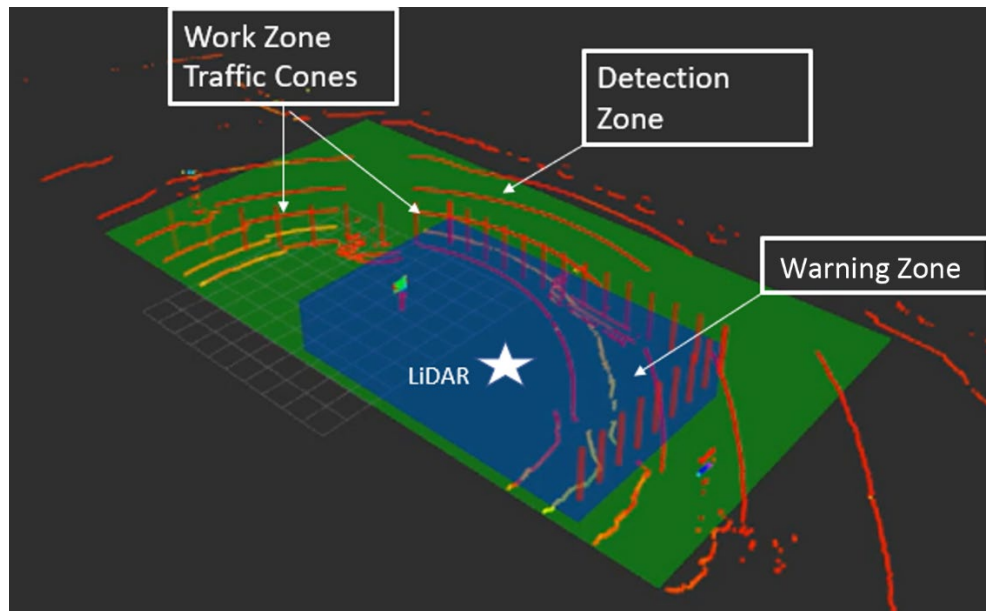
Figure 14. Diagram for the threat alert system.

Visualization

ROS visualization (Rviz) is an application for 3D visualizing robots, sensors, and algorithms [45]. Users can observe the robot's perspective of the real world or simulated scenario. In this study, researchers applied Rviz to visualize the LiDAR data, trajectory detection and prediction, and threat alert.

The dynamic reconfiguration function in ROS can be used to dynamically change a parameter's value while a node is operating. This package provides the ability to alter parameters on the parameter server during runtime and send that adjustment to a specific active node that requires the parameter's most recent value [46]. In the current research, the size of the work zone and the scale of images of multiple views can be adjusted when the program is running. The ability to adjust the size of the work zone provides flexibility to adapt to changing conditions or requirements. For example, if the user needs to expand or reduce the warning zone, they can easily adjust the work zone size to reflect the new requirements.

Results and Discussion

Detection Results

Researchers collected data with a VLP-16 attached to a heavy-duty tripod with spirit bubble indicators to balance the roll and pitch at two real-world test sites (Table 2). Datasets are stored for offline use in a "rosbag" format, which can later replay captured sensor data.

The first (01-TAMU) test site was an urban road intersection near TAMU at Church & University. Researchers collected LiDAR vehicle data during the day and windy conditions for about 10 minutes. The LiDAR was positioned at $D_h = 5.0$; $D_v = 2.2$ m. The second test site (02-TAMU) was collected during the day on a highway SH-21 near the RELLIS Campus. For safety reasons, the LiDAR was positioned further back at $D_h = 8.3$ m; $D_v = 2.2$ m. Compared to the urban scenario, the point cloud for the highway was much sparser. This was due to both the LiDAR being located further away and the high vehicle speeds (75 mph / 120 kph) resulting in shorter detections.

Researchers tested rosbags offline on two machines to evaluate the performance: (1) a mobile laptop with an Intel i7-8750H @ 3.9 GHz, and (2) a Raspberry Pi 4 with a Quad Cortex A72 @ 1.5 GHz. Relevant statistics and run-time performance were measured on a frame-by-frame basis, with averaged results presented.

For the detection results (Table 3), researchers observed the precision, recall, and mean Intersection Over Union (mIOU) averaged over a frame-by-frame basis. We observed these metrics in the context of the annotated LiDAR BeV images. In 01-TAMU, there was a very high precision where 99.5% of the detections were present in the annotations. Most instances of false-positives/false-negatives were due to over/under clustering, respectively. The mIOU score (i.e., the averaged intersection over union) was around 60% to 65% in both datasets. The remaining 40% error is majorly attributed to misclustering in vehicles with sparse LiDAR returns and marginally due to small error offsets in annotations. The small performance increases in most metrics for 02-TAMU may be attributed to the lower number of vehicles per frame. The background filtering, image generation, detection, and tracking processes were all within the 100 ms target time (for $\omega = 10$ Hz) on the i7 laptop. However, in instances with four or more vehicles in a frame, the computation time on the Raspberry Pi platform was >100 ms. Further improvements can be made by transitioning the detection code into C++ from Python.

Table 2. Background Filtering Results [33]

Dataset	Avg. error [%]	exec time [ms]	Avg. False Positive [%]	Avg. False Positive [pts]
01_TAMU	0.50	1.90	1.08	60.60
02_TAMU	0.88	1.00	2.18	119.10

Dataset	Precision	Recall	mIOU	Avg. exec time [ms]	per cluster [ms]
01_TAMU	99.5%	93.9%	58.5%	8.25	3.24
02_TAMU	100.0%	96.3%	66.7%	5.38	4.90

Trajectory Prediction/Alerting

Figure 15a shows the trajectory tracking and prediction results. The vehicle is bounded by a box, and five frames of the vehicle's future trajectory are predicted (as shown by cyan color dots). Figure 15b shows the threat alert response. When a vehicle reaches the edge of the warning zone, a message "warning" appears (shown in red). When the vehicle leaves, the threat alert disappears.
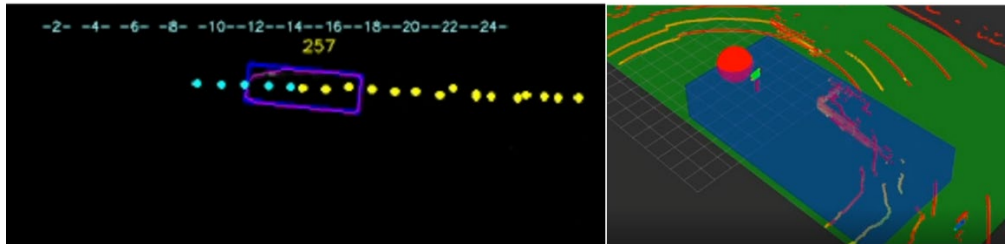
Figure 15. Graph and diagram. Threat detection and alarm: a) Trajectory and predicted path of the vehicle. b) Visualization of threat alert.

The Rviz interface displays the LiDAR data and how the system works (Figure 16). The box in the center shows a 3D view within the detection zone including the work zone LiDAR point cloud data. Three windows on the left visualize the top view, the centroid of moving objects, and trajectory tracking and prediction. With the dynamic reconfiguration, the size of the work zone and the detection zone can be adjusted.
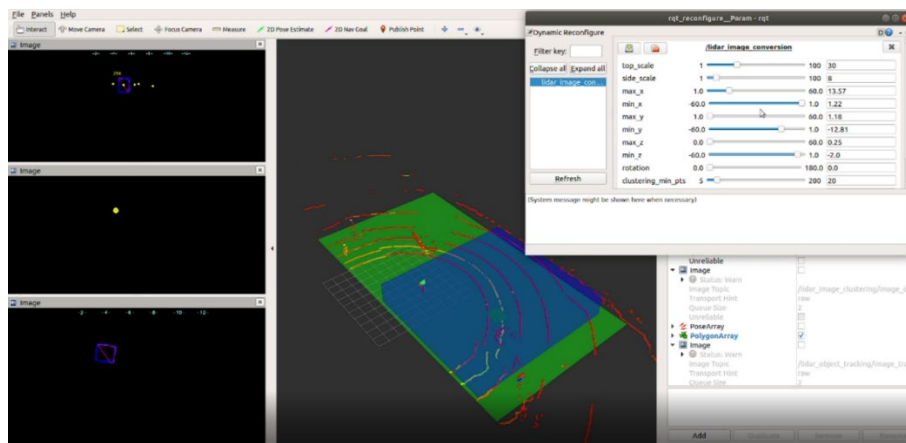
Figure 16. Screen shot. Rviz interface of the threat alert system.

Researchers tracked and predicted the trajectories of 184 vehicles; 176 of them are accurate, and eight are inaccurate. The accuracy of tracking and prediction is 95.65%. There are a few reasons that explain the threat alert errors:

- Complex driving scenarios: Trajectory prediction assumes that the vehicle will continue to behave in a predictable manner. However, complex driving scenarios like sudden stops or sharp turns can make trajectory prediction challenging.
- Model assumptions: The Kalman filter algorithm assumes that the system dynamics and sensor noise are normally distributed and linear. However, in real-world scenarios, the behavior of vehicles and sensor noise may not always follow a linear or normal distribution. In such cases, the accuracy of the Kalman filter algorithm may be limited.
- Object clustering algorithms: Object clustering algorithms could lead to incorrect or delayed threat alerts. DBSCAN, like any clustering algorithm, is designed to group similar data points based on the maximum distance between points and the minimum number of clustering data points. The accuracy of object clustering being 90%+ could result in incorrect threat alerts. For example, if the algorithm is not sensitive enough, it may fail to detect clusters or objects actually approaching the work zone, resulting in delayed alerts.

The result of threat alert appears in Table 4. In the 147 related threat information recorded, 119 are reported accurately; 25 of the threat information are not actual threats but are predicted as threats by the system. The system also considers three of them as not threats (False Positive). Overall, the system has an accuracy of 80.95%.

Table 4. Accuracy of the Intrusion Alerting

Ground truth			
		TRUE	FALSE
Prediction	TRUE	**119**	25
	FALSE	3	/

There are a several reasons that explain the threat alert errors:

- System delay can impact the accuracy and timeliness of threat alerts. Processing time varies based on algorithm complexity, computational resources, and LiDAR data size. This delay occurs between receiving LiDAR data and generating alerts.
- Vehicle speed is a significant factor in providing timely and accurate threat alerts. The LiDAR sensor in this study effectively detects up to 30 m. High-speed approaching vehicles reduce the system's time to detect and respond to potential threats. Quick vehicle arrival at the work zone necessitates rapid threat detection and response.
- Incorrect or delayed threat alerts can result from object clustering algorithms. DBSCAN clusters similar data points based on distance and minimum cluster size. With a 90% clustering accuracy, there may be incorrect alerts. Insensitivity in the algorithm could fail to detect approaching object clusters, leading to delayed alerts.

Future Research

In this study, researchers developed a prototype for a work zone vehicle intrusion/alerting system by using roadside LiDAR, which helps improve safety for workers. However, this study still has a few limitations.

Currently, the alert system can only show incoming threats that can be displayed on a device in the work zone. As we know, the velocity of vehicles is sometimes very high, and traffic crashes can happen in just seconds. Displaying threat information in a particular spot in the work zone is probably not effective enough for workers to see and react. We will further refine the alert function, and one of the solutions is to connect the threat alert to a wearable device such as a vest. When the potential threat is found, the signal will be sent and displayed to individual workers directly on their wearable devices. This measure will improve efficiency and make more time for workers to escape from danger.

Also, the detection scope in this research is another limitation. The effective detecting and tracking distance for the device is 30 m, which is not enough to monitor the traffic condition and alert all threats in advance, especially for the potential vehicle threats with high speed on highways. We will apply better LiDAR devices to collect data with a larger range in the future. Furthermore, it is not our goal to do individual research, gather information, and analyze results in a specific location. We hope the information we gain and process via the LiDAR sensor can be connected and incorporated into the traffic information platform as a helpful tool to monitor the traffic condition around the work zone in real time.

There are also other relevant research questions that warrant further examination:

1) The system has been tested in a two-lane work zone (one lane closure for construction). It would be beneficial to expand the test to more complicated roadway and work zone configurations (e.g., four-lane undivided road, freeway).
2) The system should also be tested in extreme weather events to see the tolerance of LiDAR sensors in extreme conditions (e.g., rain, snow, maximum temperature).
3) The system and algorithms can be further refined by fusing the data from multiple LiDAR sensors (at least two) to reduce occlusion and to increase the warning lead time.

Additional Products

Education and Workforce Development Products

Within the scope of this project, a master's student demonstrated commendable achievement by successfully completing their thesis, which focused on the project's central topic. Furthermore, two undergraduate students enthusiastically engaged in the project, acquiring valuable learning

experience. Additionally, a Ph.D. student made substantial contributions to the project, significantly expanding their knowledge and establishing a foundation for future research.

Technology Transfer Products

1) IEEE International Intelligent Transportation Systems Conference 2021 (September 2021): "Building a Smart Work Zone Using Roadside LiDAR"
2) TAMU Transportation Data Science Seminar Series (August 26, 2021): "Building a Smart Work Zone Using Roadside LiDAR"
3) TexITE Webinar Series, "ITS, TSMO and Big Data" (August 27, 2021): "Building a Roadside LiDAR Based Intrusion Alerting System to Improve Work Zone Safety"
4) TAMU Design & Analytics for Urban Artificial Intelligence Workshop (June 2022): "Leveraging Emerging Data and AI Technologies to Enhance Transportation Infrastructures"
5) Transportation Research Board (TRB) Annual Conference (January 2022): "Simulation of Roadside LiDAR Applications: A Smart Work Zone Case Study"
6) IEEE Sensors Conference (October 2022): "An Automatic Lane Marking Detection Method with Low-Density Roadside LiDAR Data"
7) University of Texas at Arlington Presentation (Nov. 2022): "Development of a Roadside LiDAR Based Vehicle Intrusion Altering System for Work Zones"
8) ASCE International Conference on Transportation & Development 2023 (June 2023): "Development of a Roadside LiDAR Based Situational Awareness System to Improve Work Zone Safety: A Pilot Study"
9) TRB Annual Conference (to be planned): "Development of a Roadside LiDAR Based Situational Awareness System to Improve Work Zone Safety: A Pilot Study"

Data Products

The LiDAR datasets will be uploaded to the Safe-D data portal.

References

[1]   L. Blincoe, T. Miller, E. Zaloshnja, and B. Lawrence, *The Economic and Societal Impact of Motor Vehicle Crashes, 2010*, vol. 30. 2014.

[2]   "Work Zone Traffic Crash Trends and Statistics," *Work Zone Safety Information Clearinghouse*. https://workzonesafety.org/work-zone-data/work-zone-traffic-crash-trends-and-statistics/ (accessed Apr. 03, 2023).

[3]   M. D. Finley, G. L. Ullman, J. E. Bryden, R. Srinivasan, and F. M. Council, *Traffic Safety Evaluation of Nighttime and Daytime Work Zones*. Washington, D.C.: National Academies Press, 2008. doi: 10.17226/14196.

[4]   X. Wang, R. Katz, and X. Dong, "Fatal Injuries at Road Construction Sites among Construction Workers CPWR Data Center," Jul. 2018.

[5]   T. Ore and D. E. Fosbroke, "Motor vehicle fatalities in the United States construction industry," *Accident Analysis & Prevention*, vol. 29, no. 5, pp. 613–626, Sep. 1997, doi: 10.1016/S0001-4575(97)00013-4.

[6]   S. G. Pratt, D. E. Fosbroke, and S. M. Marsh, "Building safer highway work zones : measures to prevent worker injuries from vehicles and equipment," 2001–128, Apr. 2001. Accessed: Apr. 05, 2023. [Online]. Available: https://rosap.ntl.bts.gov/view/dot/34163

[7]   E. Marks, S. C. Vereen, I. Awolusi, and University Transportation Center for Alabama, "Active Work Zone Safety Using Emerging Technologies 2017.," FHWA/CA/OR-, Jul. 2017. Accessed: Mar. 03, 2023. [Online]. Available: https://rosap.ntl.bts.gov/view/dot/32769

[8]   M.-H. Wang, S. D. Schrock, Y. Bai, R. A. Rescot, and E. and A. E. University of Kansas. Dept. of Civil, "Evaluation of innovative traffic safety devices at short-term work zones.," K-TRAN: KU-09-5R, Aug. 2013. Accessed: Mar. 03, 2023. [Online]. Available: https://rosap.ntl.bts.gov/view/dot/26339

[9]   K. R. Agent and J. O. Hibbs, "Evaluation of SHRP work zone safety devices," 1996.

[10]   J. A. Gambatese, H. W. Lee, and C. A. Nnaji, "Work zone intrusion alert technologies: Assessment and practical guidance," Oregon. Dept. of Transportation. Research Section, 2017.

[11]   L. Osborne, Y. Xiao, and S. Guizani, "Intrusion Detection Techniques in Mobile Ad Hoc and Wireless Sensor Networks," *Wireless Communications, IEEE*, vol. 14, pp. 56–63, Nov. 2007, doi: 10.1109/MWC.2007.4396943.

[12]   W. Han, E. White, M. Mollenhauer, and N. Roofigari-Esfahan, "A Connected Work Zone Hazard Detection System for Roadway Construction Workers," pp. 242–250, Jun. 2019, doi: 10.1061/9780784482445.031.

[13]   J. Park, X. Yang, Y. Cho, and J. Seo, "Improving dynamic proximity sensing and processing for smart work-zone safety," *Automation in Construction*, vol. 84, pp. 111–120, Dec. 2017, doi: 10.1016/j.autcon.2017.08.025.

[14]   N. Pradhananga and J. Teizer, "Automatic spatio-temporal analysis of construction site equipment operations using GPS data," *Automation in Construction*, vol. 29, pp. 107–122, Jan. 2013, doi: 10.1016/j.autcon.2012.09.004.

[15]   J. Park, E. Marks, Y. Cho, and W. Suryanto, "Performance Test of Wireless Technologies for Personnel and Equipment Proximity Sensing in Work Zones," *Journal of Construction Engineering and Management*, vol. 142, p. 04015049, Jul. 2015, doi: 10.1061/(ASCE)CO.1943-7862.0001031.

[16] J. M. Sullivan, "Work-zone safety ITS: smart barrel for an adaptive queue-warning system," University of Michigan, Ann Arbor, Transportation Research Institute, Technical Report, Feb. 2005. Accessed: Jun. 13, 2023. [Online]. Available: http://deepblue.lib.umich.edu/handle/2027.42/3139

[17] A. Jafarnejad, J. Gambatese, and S. Hernandez, "Influence of Truck-Mounted Radar Speed Signs in Controlling Vehicle Speed for Mobile Maintenance Operations: Oregon Case Study," *Transportation Research Record*, vol. 2617, no. 1, pp. 19–26, Jan. 2017, doi: 10.3141/2617-03.

[18] J. A. Epps and M. Ardila-Coulson, "Summary Of SHRP Research And Economic Benefits Of Work Zone Safety," FHWA-SA-98-016, Dec. 1997. Accessed: Jun. 13, 2023. [Online]. Available: https://rosap.ntl.bts.gov/view/dot/14138

[19] Y. Tsai, *Development of a Sensing Methodology for Intelligent and Reliable Work-Zone Hazard Awareness*. IDEA Program, Transportation Research Board of the National Academies, 2011.

[20] J. Teizer and P. A. Vela, "Personnel tracking on construction sites using video cameras," *Advanced Engineering Informatics*, vol. 23, pp. 452–462, Oct. 2009, doi: 10.1016/j.aei.2009.06.011.

[21] C. Lin, H. Liu, D. Wu, and B. Gong, "Background Point Filtering of Low-Channel Infrastructure-Based LiDAR Data Using a Slice-Based Projection Filtering Algorithm," *Sensors*, vol. 20, no. 11, Art. no. 11, Jan. 2020, doi: 10.3390/s20113054.

[22] D. Wu, A. Darwesh, M. Le, and S. Saripalli, "Simulation of Roadside LiDAR Applications: A Smart Work Zone Case Study," presented at the Transportation Research Board 101st Annual MeetingTransportation Research Board, 2022. Accessed: Jun. 15, 2023. [Online]. Available: https://trid.trb.org/view/1996312

[23] L. Caltagirone, M. Bellone, L. Svensson, and M. Wahde, "LIDAR–camera fusion for road detection using fully convolutional neural networks," *Robotics and Autonomous Systems*, vol. 111, pp. 125–131, 2019.

[24] C. Lin, Y. Guo, W. Li, H. Liu, and D. Wu, "An Automatic Lane Marking Detection Method With Low-Density Roadside LiDAR Data," *IEEE Sensors Journal*, vol. 21, no. 8, pp. 10029–10038, 2021.

[25] H. Liu, C. Lin, D. Wu, and B. Gong, "Slice-based instance and semantic segmentation for low-channel roadside LiDAR data," *Remote Sensing*, vol. 12, no. 22, p. 3830, 2020.

[26] "Development of a Roadside LiDAR-Based Situational Awareness System for Work Zone Safety: Proof-of-Concept Study | Safe-D: Safety through Disruption." https://safed.vtti.vt.edu/projects/development-of-a-roadside-lidar-based-situational-awareness-system-for-work-zone-safety-proof-of-concept-study/ (accessed Jul. 31, 2021).

[27] "Chattanooga DoT deploys digital lidar to improve pedestrian safety," *Ouster*. https://ouster.com/blog/chattanooga-dot-deploys-digital-lidar-to-improve-pedestrian-safety (accessed Jul. 31, 2021).

[28] "Velodyne Lidar Powering Intelligent Traffic Management in Nevada," *Velodyne Lidar*. https://velodynelidar.com/press-release/velodyne-lidar-university-nevada-reno-transportation-infrastructure/ (accessed Jul. 31, 2021).

[29] "Pedestrian behavior study to advance pedestrian safety in smart transportation systems using innovative LIDAR sensors," //, Accessed: Jul. 31, 2021. [Online]. Available: https://rip.trb.org/view/1724535

[30] "Traffic Sensor | smartmicro." https://www.smartmicro.com/traffic-sensor (accessed Jun. 13, 2023).

[31] S. Sivaraman and M. Trivedi, "Looking at Vehicles on the Road: A Survey of Vision-Based Vehicle Detection, Tracking, and Behavior Analysis," *Intelligent Transportation Systems, IEEE Transactions on*, vol. 14, pp. 1773–1795, Dec. 2013, doi: 10.1109/TITS.2013.2266661.

[32] D. Arditi, D.-E. Lee, and G. Polat, "Fatal accidents in nighttime vs. daytime highway construction work zones," *J Safety Res*, vol. 38, no. 4, pp. 399–405, 2007, doi: 10.1016/j.jsr.2007.04.001.

[33] A. Darwesh, D. Wu, M. Le, S. Saripalli, Virginia Tech Transportation Institute, and Safety through Disruption (Safe-D) University Transportation Center (UTC), "Building a Smart Work Zone Using Roadside LiDAR," Jan. 01, 2021. Accessed: Mar. 14, 2023. [Online]. Available: https://rosap.ntl.bts.gov/view/dot/60121

[34] "ROS: Home." https://www.ros.org/ (accessed Jun. 13, 2023).

[35] R. B. Rusu and S. Cousins, "3D is here: Point Cloud Library (PCL)," in *2011 IEEE International Conference on Robotics and Automation*, May 2011, pp. 1–4. doi: 10.1109/ICRA.2011.5980567.

[36] G. Bradski, *The Opencv Library*, vol. 25. 2000.

[37] W. Xiao, B. Vallet, K. Schindler, and N. Paparoditis, "SIMULTANEOUS DETECTION AND TRACKING OF PEDESTRIAN FROM PANORAMIC LASER SCANNING DATA," *ISPRS Annals of the Photogrammetry, Remote Sensing and Spatial Information Sciences*, vol. III–3, pp. 295–302, Jun. 2016, doi: 10.5194/isprs-annals-III-3-295-2016.

[38] J. Zhao, "Exploring the fundamentals of using infrastructure-based LiDAR sensors to develop connected intersections," Thesis, 2019. Accessed: Jun. 13, 2023. [Online]. Available: https://ttu-ir.tdl.org/handle/2346/85580

[39] N. M. Dzung, "Super Fast and Accurate 3D Object Detection based on 3D LiDAR Point Clouds (SFA3D)." Jun. 13, 2023. Accessed: Jun. 13, 2023. [Online]. Available: https://github.com/maudzung/SFA3D

[40] Z. Zhang, J. Zheng, H. Xu, and X. Wang, "Vehicle Detection and Tracking in Complex Traffic Circumstances with Roadside LiDAR," *Transportation Research Record*, vol. 2673, no. 9, pp. 62–71, Sep. 2019, doi: 10.1177/0361198119844457.

[41] J. Zhang, W. Xiao, B. Coifman, and J. P. Mills, "Vehicle Tracking and Speed Estimation From Roadside Lidar," *IEEE J. Sel. Top. Appl. Earth Observations Remote Sensing*, vol. 13, pp. 5597–5608, 2020, doi: 10.1109/JSTARS.2020.3024921.

[42] Y. bar-shalom, F. Daum, and J. Huang, "The probabilistic data association filter," *Control Systems, IEEE*, vol. 29, pp. 82–100, Jan. 2010, doi: 10.1109/MCS.2009.934469.

[43] J. Munkres, "Algorithms for the Assignment and Transportation Problems," *Journal of the Society for Industrial and Applied Mathematics*, vol. 5, no. 1, pp. 32–38, 1957.

[44] R. J. Meinhold and N. D. Singpurwalla, "Understanding the Kalman Filter," *The American Statistician*, vol. 37, no. 2, pp. 123–127, May 1983, doi: 10.1080/00031305.1983.10482723.

[45] "rviz - ROS Wiki." http://wiki.ros.org/rviz (accessed Dec. 10, 2022).

[46] "dynamic_reconfigure - ROS Wiki." http://wiki.ros.org/dynamic_reconfigure (accessed Dec. 10, 2022).

[47] N. J. Garber and M. Zhao, "Distribution and Characteristics of Crashes at Different Work Zone Locations in Virginia," *Transportation Research Record*, vol. 1794, no. 1, pp. 19–25, Jan. 2002, doi: 10.3141/1794-03.

[48] B. Mataei, H. Zakeri, M. Zahedi, and F. M. Nejad, "Pavement Friction and Skid Resistance Measurement Methods: A Literature Review," *Open Journal of Civil Engineering*, vol. 06, no. 04, Art. no. 04, 2016, doi: 10.4236/ojce.2016.64046.

[49] R. Hussain and S. Zeadally, "Autonomous Cars: Research Results, Issues, and Future Challenges," *IEEE Communications Surveys & Tutorials*, vol. 21, no. 2, pp. 1275–1313, 2019, doi: 10.1109/COMST.2018.2869360.

[50] R. D. Blomberg, R. C. Peck, H. Moskowitz, M. Burns, and D. Fiorentino, "The Long Beach/Fort Lauderdale relative risk study," *Journal of Safety Research*, vol. 40, pp. 285–292, 2009, doi: 10.1016/j.jsr.2009.07.002.

[51] R. Harb, E. Radwan, X. Yan, A. Pande, and M. Abdel-Aty, "Freeway Work-Zone Crash Analysis and Risk Identification Using Multiple and Conditional Logistic Regression," *Journal of Transportation Engineering*, vol. 134, no. 5, pp. 203–214, May 2008, doi: 10.1061/(ASCE)0733-947X(2008)134:5(203).

[52] Y. Peng, M. Abdel-Aty, Q. Shi, and R. Yu, "Assessing the impact of reduced visibility on traffic crash risk using microscopic data and surrogate safety measures," *Transportation Research Part C: Emerging Technologies*, vol. 74, pp. 295–305, Jan. 2017, doi: 10.1016/j.trc.2016.11.022.

[53] C. Nnaji, J. Gambatese, H. W. Lee, and F. Zhang, "Improving construction work zone safety using technology: A systematic review of applicable technologies," *Journal of Traffic and Transportation Engineering (English Edition)*, vol. 7, no. 1, pp. 61–75, Feb. 2020, doi: 10.1016/j.jtte.2019.11.001.

[54] K.-F. Wu and P. P. Jovanis, "Crashes and crash-surrogate events: Exploratory modeling with naturalistic driving data," *Accident Analysis & Prevention*, vol. 45, pp. 507–516, Mar. 2012, doi: 10.1016/j.aap.2011.09.002.

[55] A. K. Debnath, R. Blackman, and N. Haworth, "Common hazards and their mitigating measures in work zones: A qualitative study of worker perceptions," *Safety Science*, vol. 72, pp. 293–301, Feb. 2015, doi: 10.1016/j.ssci.2014.09.022.

[56] H. Yang, K. Ozbay, O. Ozturk, and K. Xie, "Work Zone Safety Analysis and Modeling: A State-of-the-Art Review," *Traffic Injury Prevention*, vol. 16, no. 4, pp. 387–396, May 2015, doi: 10.1080/15389588.2014.948615.

[57] E. Marks and J. Teizer, "Proximity Sensing and Warning Technology for Heavy Construction Equipment Operation," pp. 981–990, Jul. 2012, doi: 10.1061/9780784412329.099.

[58] P. García-Teodoro, J. Díaz-Verdejo, G. Maciá-Fernández, and E. Vázquez, "Anomaly-based network intrusion detection: Techniques, systems and challenges," *Computers & Security*, vol. 28, no. 1, pp. 18–28, Feb. 2009, doi: 10.1016/j.cose.2008.08.003.

[59] S. Olariu and M. C. Weigle, Eds., *Vehicular Networks: From Theory to Practice*. New York: Chapman and Hall/CRC, 2009. doi: 10.1201/9781420085891.

[60] W. Umer and M. K. Siddiqui, "Use of Ultra Wide Band Real-Time Location System on Construction Jobsites: Feasibility Study and Deployment Alternatives," *Int J Environ Res Public Health*, vol. 17, no. 7, p. 2219, Apr. 2020, doi: 10.3390/ijerph17072219.

[61]   P. Vanin *et al.*, "A Study of Network Intrusion Detection Systems Using Artificial Intelligence/Machine Learning," *Applied Sciences*, vol. 12, no. 22, Art. no. 22, Jan. 2022, doi: 10.3390/app122211752.

[62]   P. Sun, C. Sun, R. Wang, and X. Zhao, "Object Detection Based on Roadside LiDAR for Cooperative Driving Automation: A Review," *Sensors*, vol. 22, no. 23, Art. no. 23, Jan. 2022, doi: 10.3390/s22239316.

[63]   C. Lin, H. Zhang, B. Gong, D. Wu, and Y.-J. Wang, "Density variation-based background filtering algorithm for low-channel roadside lidar data," *Optics & Laser Technology*, vol. 158, p. 108852, Feb. 2023, doi: 10.1016/j.optlastec.2022.108852.

[64]   J. Zhao, H. Xu, Z. Chen, and H. Liu, "A decoding-based method for fast background filtering of roadside LiDAR data," *Advanced Engineering Informatics*, vol. 57, p. 102043, Aug. 2023, doi: 10.1016/j.aei.2023.102043.

[65]   J. Wu, H. Xu, Y. Zheng, and Z. Tian, "A novel method of vehicle-pedestrian near-crash identification with roadside LiDAR data," *Accident Analysis & Prevention*, vol. 121, pp. 238–249, Dec. 2018, doi: 10.1016/j.aap.2018.09.001.

[66]   J. Zhao, H. Xu, X. Xia, and H. Liu, "Azimuth-Height Background Filtering Method for Roadside LiDAR Data," in *2019 IEEE Intelligent Transportation Systems Conference (ITSC)*, Oct. 2019, pp. 2421–2426. doi: 10.1109/ITSC.2019.8917369.

[67]   Z. Zhang, J. Zheng, X. Wang, and X. Fan, "Background Filtering and Vehicle Detection with Roadside Lidar Based on Point Association," in *2018 37th Chinese Control Conference (CCC)*, Jul. 2018, pp. 7938–7943. doi: 10.23919/ChiCC.2018.8484040.

[68]   Y. Zhang, H. Xu, and J. Wu, "An Automatic Background Filtering Method for Detection of Road Users in Heavy Traffics Using Roadside 3-D LiDAR Sensors With Noises," *IEEE Sensors Journal*, vol. 20, no. 12, pp. 6596–6604, Jun. 2020, doi: 10.1109/JSEN.2020.2976663.

[69]   Z. Zhang, J. Zheng, H. Xu, X. Wang, X. Fan, and R. Chen, "Automatic Background Construction and Object Detection Based on Roadside LiDAR," *IEEE Transactions on Intelligent Transportation Systems*, vol. 21, no. 10, pp. 4086–4097, Oct. 2020, doi: 10.1109/TITS.2019.2936498.

[70]   Y. Cui, H. Xu, J. Wu, Y. Sun, and J. Zhao, "Automatic Vehicle Tracking With Roadside LiDAR Data for the Connected-Vehicles System," *IEEE Intelligent Systems*, vol. 34, no. 3, pp. 44–51, May 2019, doi: 10.1109/MIS.2019.2918115.

[71]   J. Wu, H. Xu, and J. Zheng, "Automatic background filtering and lane identification with roadside LiDAR data," in *2017 IEEE 20th International Conference on Intelligent Transportation Systems (ITSC)*, Yokohama, Japan: IEEE Press, Oct. 2017, pp. 1–6. doi: 10.1109/ITSC.2017.8317723.

[72]   B. Lv, H. Xu, J. Wu, Y. Tian, and C. Yuan, "Raster-Based Background Filtering for Roadside LiDAR Data," *IEEE Access*, vol. 7, pp. 76779–76788, 2019, doi: 10.1109/ACCESS.2019.2919624.

[73]   Y. Song, H. Zhang, Y. Liu, J. Liu, H. Zhang, and X. Song, "Background Filtering and Object Detection With a Stationary LiDAR Using a Layer-Based Method," *IEEE Access*, vol. 8, pp. 184426–184436, 2020, doi: 10.1109/ACCESS.2020.3029341.

[74]   J. Wu, Y. Tian, H. Xu, R. Yue, A. Wang, and X. Song, "Automatic ground points filtering of roadside LiDAR data using a channel-based filtering algorithm," *Optics & Laser Technology*, vol. 115, pp. 374–383, Jul. 2019, doi: 10.1016/j.optlastec.2019.02.039.

[75] L. Wang and B. Goldluecke, "Sparse-PointNet: See Further in Autonomous Vehicles," *IEEE Robot. Autom. Lett.*, vol. 6, no. 4, pp. 7049–7056, Oct. 2021, doi: 10.1109/LRA.2021.3096253.

[76] A. Mammeri, T. Zuo, and A. Boukerche, "Extending the detection range of vision-based driver assistance systems application to Pedestrian Protection System," in *2014 IEEE Global Communications Conference*, Dec. 2014, pp. 1358–1363. doi: 10.1109/GLOCOM.2014.7036997.

[77] Y. Sun, H. Xu, J. Wu, J. Zheng, and K. M. Dietrich, "3-D Data Processing to Extract Vehicle Trajectories from Roadside LiDAR Data," *Transportation Research Record*, vol. 2672, no. 45, pp. 14–22, Dec. 2018, doi: 10.1177/0361198118775839.

[78] M. Ester, H. Kriegel, J. Sander, and X. Xu, "A Density-Based Algorithm for Discovering Clusters in Large Spatial Databases with Noise," presented at the Knowledge Discovery and Data Mining, Aug. 1996. Accessed: Apr. 07, 2023. [Online]. Available: https://www.semanticscholar.org/paper/A-Density-Based-Algorithm-for-Discovering-Clusters-Ester-Kriegel/5c8fe9a0412a078e30eb7e5eeb0068655b673e86

[79] N. Pfeifer, P. Stadler, and C. Briese, "DERIVATION OF DIGITAL TERRAIN MODELS IN THE SCOP++ ENVIRONMENT," 2001. Accessed: Apr. 07, 2023. [Online]. Available: https://www.semanticscholar.org/paper/DERIVATION-OF-DIGITAL-TERRAIN-MODELS-IN-THE-SCOP%2B%2B-Pfeifer-Stadler/71d326fcb19cf7ef8624e704aad50deacb89c955

[80] J. Sander, M. Ester, H.-P. Kriegel, and X. Xu, "Density-Based Clustering in Spatial Databases: The Algorithm GDBSCAN and Its Applications," *Data Mining and Knowledge Discovery*, vol. 2, no. 2, pp. 169–194, Jun. 1998, doi: 10.1023/A:1009745219419.

[81] R. J. G. B. Campello, D. Moulavi, and J. Sander, "Density-Based Clustering Based on Hierarchical Density Estimates," in *Advances in Knowledge Discovery and Data Mining*, J. Pei, V. S. Tseng, L. Cao, H. Motoda, and G. Xu, Eds., in Lecture Notes in Computer Science. Berlin, Heidelberg: Springer, 2013, pp. 160–172. doi: 10.1007/978-3-642-37456-2_14.

[82] V. N. Vapnik, *The Nature of Statistical Learning Theory*. New York, NY: Springer, 1995. doi: 10.1007/978-1-4757-2440-0.

[83] L. Breiman, "Random Forests," *Machine Learning*, vol. 45, no. 1, pp. 5–32, Oct. 2001, doi: 10.1023/A:1010933404324.

[84] T. Chen and C. Guestrin, "XGBoost: A Scalable Tree Boosting System," in *Proceedings of the 22nd ACM SIGKDD International Conference on Knowledge Discovery and Data Mining*, in KDD '16. New York, NY, USA: Association for Computing Machinery, Aug. 2016, pp. 785–794. doi: 10.1145/2939672.2939785.

[85] Y. Freund and R. E. Schapire, "A Decision-Theoretic Generalization of On-Line Learning and an Application to Boosting," *Journal of Computer and System Sciences*, vol. 55, no. 1, pp. 119–139, Aug. 1997, doi: 10.1006/jcss.1997.1504.

[86] M. Ankerst, M. M. Breunig, H.-P. Kriegel, and J. Sander, "OPTICS: ordering points to identify the clustering structure," *SIGMOD Rec.*, vol. 28, no. 2, pp. 49–60, Jun. 1999, doi: 10.1145/304181.304187.

[87] Y. LeCun, Y. Bengio, and G. Hinton, "Deep learning," *Nature*, vol. 521, no. 7553, Art. no. 7553, May 2015, doi: 10.1038/nature14539.

[88] X. Chen, H. Ma, J. Wan, B. Li, and T. Xia, "Multi-View 3D Object Detection Network for Autonomous Driving." arXiv, Jun. 21, 2017. doi: 10.48550/arXiv.1611.07759.

[89] L. Mutanu, J. Gohil, and K. Gupta, "Vision-Autocorrect: A Self-Adapting Approach towards Relieving Eye-Strain Using Facial-Expression Recognition," *Software*, vol. 2, no. 2, Art. no. 2, Jun. 2023, doi: 10.3390/software2020009.

[90] D. Maturana and S. Scherer, "VoxNet: A 3D Convolutional Neural Network for real-time object recognition," in *2015 IEEE/RSJ International Conference on Intelligent Robots and Systems (IROS)*, Sep. 2015, pp. 922–928. doi: 10.1109/IROS.2015.7353481.

[91] C. R. Qi, L. Yi, H. Su, and L. J. Guibas, "PointNet++: Deep Hierarchical Feature Learning on Point Sets in a Metric Space," in *Advances in Neural Information Processing Systems*, Curran Associates, Inc., 2017. Accessed: Apr. 07, 2023. [Online]. Available: https://papers.nips.cc/paper_files/paper/2017/hash/d8bf84be3800d12f74d8b05e9b89836f-Abstract.html

[92] C. R. Qi, H. Su, K. Mo, and L. J. Guibas, "PointNet: Deep Learning on Point Sets for 3D Classification and Segmentation." arXiv, Apr. 10, 2017. doi: 10.48550/arXiv.1612.00593.

[93] S. Karagiannakos, "Graph Neural Networks - An overview," *AI Summer*, Feb. 01, 2020. https://theaisummer.com/Graph_Neural_Networks/ (accessed Apr. 14, 2023).

[94] A. Schweidtmann, J. Rittig, A. König, M. Grohe, A. Mitsos, and M. Dahmen, "Graph Neural Networks for Prediction of Fuel Ignition Quality." ChemRxiv, May 13, 2020. doi: 10.26434/chemrxiv.12280325.v1.

[95] C. R. Qi, X. Chen, O. Litany, and L. J. Guibas, "ImVoteNet: Boosting 3D Object Detection in Point Clouds with Image Votes." arXiv, Jan. 29, 2020. doi: 10.48550/arXiv.2001.10692.

[96] Y. Zhou and O. Tuzel, "VoxelNet: End-to-End Learning for Point Cloud Based 3D Object Detection," in *2018 IEEE/CVF Conference on Computer Vision and Pattern Recognition*, Jun. 2018, pp. 4490–4499. doi: 10.1109/CVPR.2018.00472.

[97] Y. Yan, Y. Mao, and B. Li, "SECOND: Sparsely Embedded Convolutional Detection," *Sensors*, vol. 18, no. 10, Art. no. 10, Oct. 2018, doi: 10.3390/s18103337.

[98] Y. Zhou *et al.*, "End-to-End Multi-View Fusion for 3D Object Detection in LiDAR Point Clouds," in *Proceedings of the Conference on Robot Learning*, PMLR, May 2020, pp. 923–932. Accessed: May 05, 2023. [Online]. Available: https://proceedings.mlr.press/v100/zhou20a.html

[99] B. Yan, C. Wang, G. Guo, and Y. Lou, "TinyGNN: Learning Efficient Graph Neural Networks," in *Proceedings of the 26th ACM SIGKDD International Conference on Knowledge Discovery & Data Mining*, in KDD '20. New York, NY, USA: Association for Computing Machinery, Aug. 2020, pp. 1848–1856. doi: 10.1145/3394486.3403236.

[100] C. R. Qi, O. Litany, K. He, and L. J. Guibas, "Deep Hough Voting for 3D Object Detection in Point Clouds." arXiv, Aug. 22, 2019. doi: 10.48550/arXiv.1904.09664.

[101] Z. Bai, G. Wu, X. Qi, Y. Liu, K. Oguchi, and M. J. Barth, "Infrastructure-Based Object Detection and Tracking for Cooperative Driving Automation: A Survey," in *2022 IEEE Intelligent Vehicles Symposium (IV)*, Jun. 2022, pp. 1366–1373. doi: 10.1109/IV51971.2022.9827461.

[102] P. N. F. bt Mohd Shamsuddin and M. A. bin Mansor, "Motion Control Algorithm for Path Following and Trajectory Tracking for Unmanned Surface Vehicle: A Review Paper," in *2018 3rd International Conference on Control, Robotics and Cybernetics (CRC)*, Sep. 2018, pp. 73–77. doi: 10.1109/CRC.2018.00023.

[103] F. Leon, M. Gavrilescu, and D. N. Sidorov, "A Review of Tracking and Trajectory Prediction Methods for Autonomous Driving," *Mathematics (2227-7390)*, vol. 9, no. 6, pp. 660–660, Mar. 2021, doi: 10.3390/math9060660.

[104] Z. Bai, G. Wu, X. Qi, Y. Liu, K. Oguchi, and M. J. Barth, "Infrastructure-Based Object Detection and Tracking for Cooperative Driving Automation: A Survey." arXiv, Mar. 19, 2022. doi: 10.48550/arXiv.2201.11871.

[105] J. Zhang, W. Xiao, and J. P. Mills, "Optimizing Moving Object Trajectories from Roadside Lidar Data by Joint Detection and Tracking," *Remote Sensing*, vol. 14, no. 9, Art. no. 9, Jan. 2022, doi: 10.3390/rs14092124.

[106] J. Zhao, H. Xu, J. Wu, Y. Zheng, and H. Liu, "Trajectory tracking and prediction of pedestrian's crossing intention using roadside LiDAR," *IET Intelligent Transport Systems*, vol. 13, no. 5, pp. 789–795, 2019, doi: 10.1049/iet-its.2018.5258.

[107] S. J. Julier and J. K. Uhlmann, "New extension of the Kalman filter to nonlinear systems," in *Signal Processing, Sensor Fusion, and Target Recognition VI*, SPIE, Jul. 1997, pp. 182–193. doi: 10.1117/12.280797.

[108] R. E. Kalman, "A New Approach to Linear Filtering and Prediction Problems," *Journal of Basic Engineering*, vol. 82, no. 1, pp. 35–45, Mar. 1960, doi: 10.1115/1.3662552.

[109] H. E. Emara-Shabaik and C. T. Leondes, "A note on the extended kalman filter," *Automatica*, vol. 17, no. 2, pp. 411–412, Mar. 1981, doi: 10.1016/0005-1098(81)90062-5.

[110] M. S. Arulampalam, S. Maskell, N. Gordon, and T. Clapp, "A tutorial on particle filters for online nonlinear/non-Gaussian Bayesian tracking," *IEEE Transactions on Signal Processing*, vol. 50, no. 2, pp. 174–188, Feb. 2002, doi: 10.1109/78.978374.

[111] D. Reid, "An algorithm for tracking multiple targets," *IEEE Transactions on Automatic Control*, vol. 24, no. 6, pp. 843–854, Dec. 1979, doi: 10.1109/TAC.1979.1102177.

[112] J. Dezert and Y. Bar-Shalom, "Joint probabilistic data association for autonomous navigation," *IEEE Transactions on Aerospace and Electronic Systems*, vol. 29, no. 4, pp. 1275–1286, Oct. 1993, doi: 10.1109/7.259531.

[113] H. Nam and B. Han, "Learning Multi-Domain Convolutional Neural Networks for Visual Tracking," presented at the Proceedings of the IEEE Conference on Computer Vision and Pattern Recognition, 2016, pp. 4293–4302. Accessed: Apr. 20, 2023. [Online]. Available: https://openaccess.thecvf.com/content_cvpr_2016/html/Nam_Learning_Multi-Domain_Convolutional_CVPR_2016_paper.html

[114] A. Sadeghian, A. Alahi, and S. Savarese, "Tracking the Untrackable: Learning to Track Multiple Cues With Long-Term Dependencies," presented at the Proceedings of the IEEE International Conference on Computer Vision, 2017, pp. 300–311. Accessed: Apr. 20, 2023. [Online]. Available: https://openaccess.thecvf.com/content_iccv_2017/html/Sadeghian_Tracking_the_Untrackable_ICCV_2017_paper.html

[115] L. Bertinetto, J. Valmadre, J. F. Henriques, A. Vedaldi, and P. H. S. Torr, "Fully-Convolutional Siamese Networks for Object Tracking," in *Computer Vision – ECCV 2016 Workshops*, G. Hua and H. Jégou, Eds., in Lecture Notes in Computer Science. Cham: Springer International Publishing, 2016, pp. 850–865. doi: 10.1007/978-3-319-48881-3_56.

[116] Y. Li, H. Ai, T. Yamashita, S. Lao, and M. Kawade, "Tracking in Low Frame Rate Video: A Cascade Particle Filter with Discriminative Observers of Different Life Spans," *IEEE*

Transactions on Pattern Analysis and Machine Intelligence, vol. 30, no. 10, pp. 1728–1740, Oct. 2008, doi: 10.1109/TPAMI.2008.73.

[117] M. Everingham, L. Van Gool, C. K. I. Williams, J. Winn, and A. Zisserman, "The Pascal Visual Object Classes (VOC) Challenge," *Int J Comput Vis*, vol. 88, no. 2, pp. 303–338, Jun. 2010, doi: 10.1007/s11263-009-0275-4.

[118] M. Sokolova and G. Lapalme, "A systematic analysis of performance measures for classification tasks," *Information Processing & Management*, vol. 45, no. 4, pp. 427–437, Jul. 2009, doi: 10.1016/j.ipm.2009.03.002.

[119] C. J. Willmott and K. Matsuura, "Advantages of the mean absolute error (MAE) over the root mean square error (RMSE) in assessing average model performance," *Climate Research*, vol. 30, no. 1, pp. 79–82, Dec. 2005, doi: 10.3354/cr030079.

[120] A. Wehr and U. Lohr, "Airborne laser scanning—an introduction and overview," *ISPRS Journal of Photogrammetry and Remote Sensing*, vol. 54, no. 2, pp. 68–82, Jul. 1999, doi: 10.1016/S0924-2716(99)00011-8.

[121] S. Slob and R. Hack, "3D Terrestrial Laser Scanning as a New Field Measurement and Monitoring Technique," in *Engineering Geology for Infrastructure Planning in Europe: A European Perspective*, R. Hack, R. Azzam, and R. Charlier, Eds., in Lecture Notes in Earth Sciences. Berlin, Heidelberg: Springer, 2004, pp. 179–189. doi: 10.1007/978-3-540-39918-6_22.

[122] H. Guan, J. Li, Y. Yu, M. Chapman, and C. Wang, "Automated Road Information Extraction From Mobile Laser Scanning Data," *IEEE Transactions on Intelligent Transportation Systems*, vol. 16, no. 1, pp. 194–205, Feb. 2015, doi: 10.1109/TITS.2014.2328589.

[123] H. Wang, C. Wang, and L. Xie, "Lightweight 3-D Localization and Mapping for Solid-State LiDAR," *IEEE Robotics and Automation Letters*, vol. 6, no. 2, pp. 1801–1807, Apr. 2021, doi: 10.1109/LRA.2021.3060392.

[124] I. Puente, H. González-Jorge, J. Martínez-Sánchez, and P. Arias, "Review of mobile mapping and surveying technologies," *Measurement*, vol. 46, no. 7, pp. 2127–2145, Aug. 2013, doi: 10.1016/j.measurement.2013.03.006.

[125] D. Bolkas, G. Fotopoulos, and C. Glennie, "On the impact of a refined stochastic model for airborne LiDAR measurements," *Journal of Applied Geodesy*, vol. 10, no. 3, pp. 185–196, Sep. 2016, doi: 10.1515/jag-2016-0005.

[126] A. Kamann, P. Held, F. Perras, P. Zaumseil, T. Brandmeier, and U. T. Schwarz, "Automotive Radar Multipath Propagation in Uncertain Environments," *2018 21st International Conference on Intelligent Transportation Systems (ITSC)*, pp. 859–864, Nov. 2018, doi: 10.1109/ITSC.2018.8570016.

[127] B. Höfle and N. Pfeifer, "Correction of laser scanning intensity data: Data and model-driven approaches," *ISPRS Journal of Photogrammetry and Remote Sensing*, vol. 62, no. 6, pp. 415–433, Dec. 2007, doi: 10.1016/j.isprsjprs.2007.05.008.

[128] C. Glennie and D. D. Lichti, "Static Calibration and Analysis of the Velodyne HDL-64E S2 for High Accuracy Mobile Scanning," *Remote Sensing*, vol. 2, no. 6, Art. no. 6, Jun. 2010, doi: 10.3390/rs2061610.

[129] T. Rabbani, S. Dijkman, F. van den Heuvel, and G. Vosselman, "An integrated approach for modelling and global registration of point clouds," *ISPRS Journal of Photogrammetry and Remote Sensing*, vol. 61, no. 6, pp. 355–370, Feb. 2007, doi: 10.1016/j.isprsjprs.2006.09.006.

[130] A. Habib, K. I. Bang, A. P. Kersting, and D.-C. Lee, "Error Budget of Lidar Systems and Quality Control of the Derived Data," *photogramm eng remote sensing*, vol. 75, no. 9, pp. 1093–1108, Sep. 2009, doi: 10.14358/PERS.75.9.1093.

[131] J. Skaloud and D. Lichti, "Rigorous approach to bore-sight self-calibration in airborne laser scanning," *ISPRS Journal of Photogrammetry and Remote Sensing*, vol. 61, no. 1, pp. 47–59, Oct. 2006, doi: 10.1016/j.isprsjprs.2006.07.003.

[132] M. Horton, "How to Easily Estimate Vehicle Localization Errors from IMU Specs," *ANELLO Photonics*, Mar. 01, 2023. https://medium.com/anello-photonics/how-to-easily-estimate-vehicle-localization-errors-from-imu-specs-31e6174ff065 (accessed Jun. 15, 2023).

[133] K. C. Chang, Y. Song, and M. E. L. Ii, "Performance modeling for multisensor data fusion," in *Signal Processing, Sensor Fusion, and Target Recognition XII*, SPIE, Aug. 2003, pp. 354–363. doi: 10.1117/12.486868.

[134] B. Khaleghi, A. Khamis, F. O. Karray, and S. N. Razavi, "Multisensor data fusion: A review of the state-of-the-art," *Information Fusion*, vol. 14, no. 1, pp. 28–44, Jan. 2013, doi: 10.1016/j.inffus.2011.08.001.

[135] C.-X. Li *et al.*, "SCRATCH: A Scalable Discrete Matrix Factorization Hashing for Cross-Modal Retrieval," in *Proceedings of the 26th ACM international conference on Multimedia*, in MM '18. New York, NY, USA: Association for Computing Machinery, Oct. 2018, pp. 1–9. doi: 10.1145/3240508.3240547.

[136] B. Zhang, Z. Yan, J. Wang, Y. Luo, S. Yang, and Z. Fei, "An Audio-Visual Quality Assessment Methodology in Virtual Reality Environment," in *2018 IEEE International Conference on Multimedia & Expo Workshops (ICMEW)*, Jul. 2018, pp. 1–6. doi: 10.1109/ICMEW.2018.8551522.

[137] "Automated Driving Toolbox." https://www.mathworks.com/products/automated-driving.html (accessed Jul. 31, 2021).

Appendix A: Literature Review

Work Zone Safety

Work zone crashes can be attributed to various factors, which can be broadly categorized into human-related factors and environmental or external factors. Understanding these causes can help mitigate the risks associated with work zones.

Human-Related Factors:

- Driver inattention: As previously mentioned, driver inattention is a significant cause of work zone crashes, with distractions leading to slower reaction times [47].
- Speeding: Driving at excessive speeds in work zones increases the likelihood of collisions due to reduced reaction time and increased stopping distance [48].
- Aggressive driving: Aggressive behaviors, such as tailgating, sudden lane changes, and frequent acceleration or deceleration, can lead to crashes in work zones [49].
- Impaired driving: Driving under the influence of alcohol or drugs severely impairs a driver's ability to safely navigate work zones, resulting in an increased risk of crashes [50].

Environmental or External Factors:

- Work zone design: Poorly designed or maintained work zones with unclear signage, insufficient lighting, or inadequate lane markings can cause confusion and increase the risk of crashes [51].
- Construction equipment and workers: The presence of construction equipment and workers in work zones creates additional hazards for drivers, who may be unfamiliar with the movements and operations of such machinery [6].
- Weather conditions: Adverse weather conditions, such as rain, fog, or snow, can reduce visibility and create hazardous driving conditions in work zones [52].
- Road surface conditions: Uneven or slippery road surfaces due to construction activity or weather can cause drivers to lose control of their vehicles, resulting in crashes [48].

Methods to Improve Work Zone Safety

Improving work zone safety requires a multifaceted approach that addresses various aspects; the methods are list below:

- Engineering: Implementing proper work zone design and traffic control can help reduce the risk of crashes. This includes using clear signage, adequate lighting, and well-defined lane markings. Additionally, portable barriers and rumble strips can help channel traffic and alert drivers to changing conditions [53].
- Enforcement: Strict enforcement of work zone regulations, such as speed limits and lane restrictions, can deter unsafe driving behaviors. Automated enforcement systems, like speed cameras, can be used to supplement traditional police enforcement [54].

- Education: Public awareness campaigns and driver education programs can help drivers understand the risks associated with work zones and promote safe driving behaviors [55].

Despite the potential benefits of these measures, they also have limitations. Engineering solutions can be costly to implement and maintain, and they may not fully address issues related to driver behavior or unforeseen circumstances. Enforcement efforts can be resource-intensive, and public acceptance of automated enforcement systems may be limited due to privacy concerns. The effectiveness of education measures may be limited by drivers' willingness to change their behaviors and the difficulty of reaching all drivers with the intended message. Figure 17 shows the effectiveness of different types of work zone safety controls.
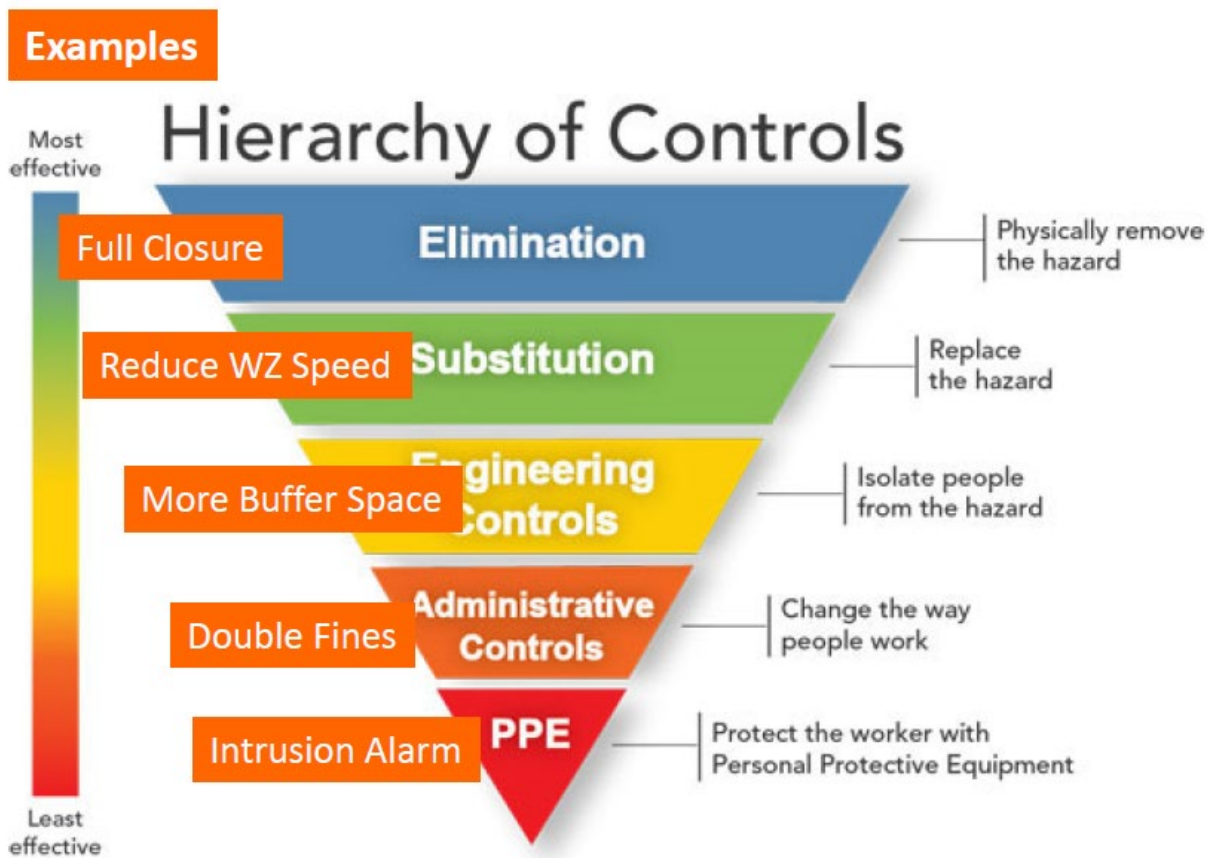
Figure 17. Diagram. Effectiveness of different types of controls (Source: CDC).

WZIAS

WZIAS are safety technologies designed to monitor and detect unauthorized vehicles, pedestrians, or objects entering a designated work zone. These systems provide real-time alerts to construction crews and supervisors, allowing them to respond quickly to potentially dangerous situations [53]. WZIAS aim to reduce the risk of crashes, injuries, and fatalities in work zones.

- **Enhancing safety:** WZIAS help protect construction workers, drivers, and pedestrians by providing real-time alerts and warnings about potential hazards in work zones. By detecting

intrusions and alerting those in the vicinity, these systems help prevent crashes and save lives.

- **Reducing crashes:** Work zones often have reduced speed limits, lane closures, and other changes in traffic patterns that can lead to increased crashes [56]. By monitoring and managing work zones using WZIAS, the number of crashes can be significantly reduced.

- **Improving work zone management:** WZIAS can improve work zone management by providing real-time data on traffic conditions, worker locations, and equipment status [57]. This information can be used to optimize work zone layouts, scheduling, and overall operations, leading to more efficient project delivery.

- **Enhancing public perception:** WZIAS can contribute to positive public perception by demonstrating that transportation agencies are proactive in implementing safety measures to protect workers and the public. Improved public perception can lead to increased support for infrastructure projects and funding.

The development of WZIAS can be traced back to the growing awareness of work zone safety issues and the need to protect construction crews from crashes. Their development has been a gradual process, driven by advancements in technology and research on work zone safety. In the early 1990s, the focus on work zone safety increased as the Federal Highway Administration began emphasizing the importance of reducing work zone fatalities and injuries [8]. This led to the development of various traffic control devices and technologies aimed at improving work zone safety, including intrusion alarm systems. Initial work zone intrusion detection systems utilized sensors and alarms, which were designed to alert construction workers of unauthorized intrusions by vehicles or pedestrians [58]. These early systems faced challenges in terms of reliability and false alarms, prompting further research and development. Over the years, advancements in technology have led to the improvement of WZIAS. For example, the introduction of radar and wireless technologies has improved the accuracy and effectiveness of intrusion detection systems [59]. Additionally, the integration of GPS and other location-based technologies has further enhanced the ability of WZIAS to provide real-time alerts to construction crews and supervisors [60]. As research on work zone safety continues, new technologies and strategies are being developed and refined to improve WZIAS. For instance, the use of artificial intelligence and machine learning algorithms may further enhance the effectiveness of WZIAS by reducing false alarms and increasing the accuracy of intrusion detection [61].

The systems mentioned can be categorized into three main types:

- **Mechanical systems** utilize mechanisms such as impact-activated or pressure-activated systems. These mechanisms are triggered by physical contact or impacts caused by intruding vehicles [11].
- **Electronic systems** employ various sensing technologies such as UWB [12], [13], GPS [14], RFID [15], magnetic field sensors [16], radar [17], infrared sensors [18], laser sensors [7], video cameras [19], [20], and others to detect intruding objects.

- **Dedicated observers** are individuals positioned strategically as workers or flaggers whose primary task is to identify intrusions and activate alarms [19].

Although these systems offer potential benefits, their adoption in the highway construction industry has been limited. Some concerns raised about these technologies include their effectiveness, the cost implications associated with adopting new technology, and the lack of synergy among different technological features [7]. For instance, mechanical systems have a significant limitation, as they require the operator to be present during a warning in order to notice any changes in work-zone barricade formations. On the other hand, electronic systems face challenges such as frequent false alarms and difficulties in system setup.

Roadside LiDAR Data Processing Algorithms

LiDAR technology utilizes laser beams to accurately detect and determine the positions of objects. It comprises a swiftly rotating array of detector pairs housed within a fixed structure, allowing efficient scanning of the surroundings. By emitting and receiving laser beams, LiDAR gathers highly detailed 3D information about the surrounding environment. The detection range is typically 0 to 200 meters. Each laser is fired approximately 18,000 times per second, generating a real-time stream of comprehensive 3D point data. The recorded attributes of a laser point include distance, intensity, x-coordinate, y-coordinate, z-coordinate, azimuth, and timestamp. The point cloud output from roadside LiDAR is shown in Figure 18 [62].

(a) Point clouds from a Single Roadside LiDAR Output
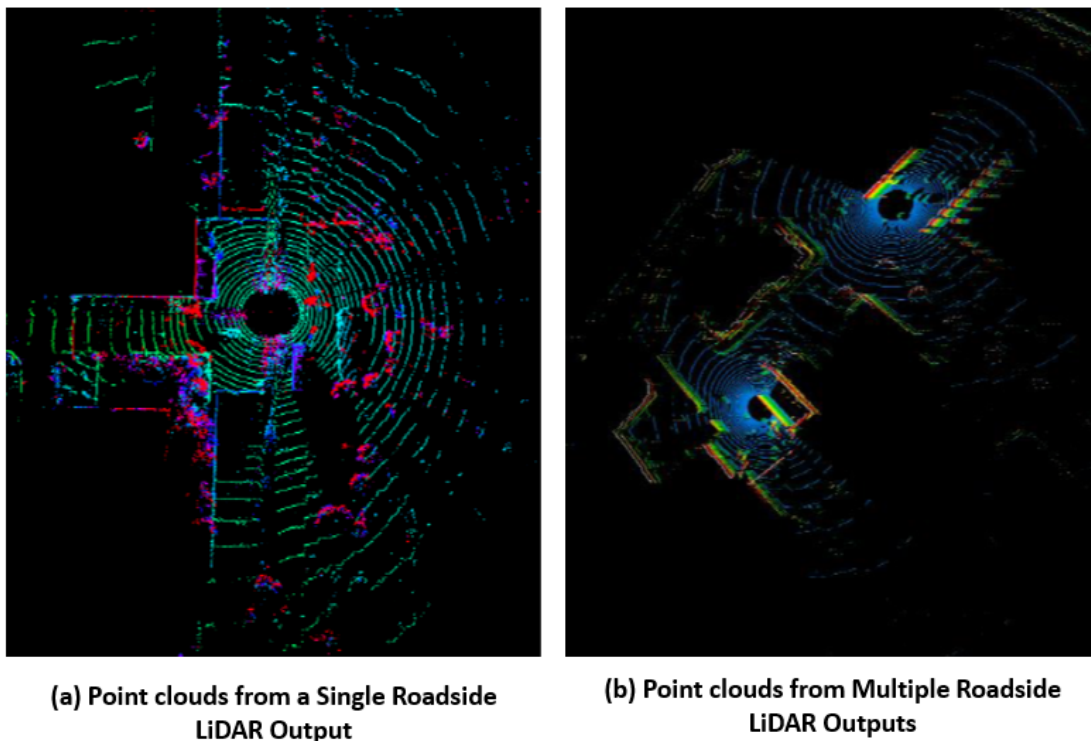
(b) Point clouds from Multiple Roadside LiDAR Outputs

Figure 18. Graphs. The output point cloud from roadside LiDAR [62].

Compared to traditional traffic detectors like video, infrared, radar, radio frequency, and geomagnetic sensors, LiDAR sensors offer a more extensive and detailed range of traffic flow characteristics and parameters. Within the scanning range of LiDAR, it becomes possible to extract high-resolution, fine-grained data regarding the position, direction, speed, and even the trajectory of each road user. The micro-level traffic data collected by a roadside LiDAR sensor holds great value as an input for various traffic applications, including vehicle-infrastructure cooperation systems, connected/autonomous vehicle systems, analysis aimed at reducing vehicle-to-pedestrian crashes, intelligent traffic signals, and other related fields [63].

The objectives and requirements for processing roadside data differ significantly from onboard LiDAR data [64]:

- Onboard LiDAR sensors, usually equipped with a minimum of 64 lasers, are mounted on moving vehicles to capture high-density point cloud data. In contrast, roadside LiDAR sensors, which are cost-effective and typically have 16 or 32 lasers, are installed on the infrastructure side. The data they capture are relatively low-density.
- Onboard LiDAR sensors primarily focus on the immediate surroundings of the vehicle. In contrast, roadside LiDAR sensors face the challenge of covering a much larger area, such as an entire intersection. Therefore, the detection and tracking task becomes more challenging for roadside LiDAR within the designated ROI.
- Onboard LiDAR sensors are commonly considered secondary sensors in autonomous vehicles. They work in conjunction with other sensors like video cameras and rely on additional data sources such as high-resolution 3D maps and GPS information. Conversely, roadside LiDAR sensors are expected to operate independently, without relying on additional sensors or data sources.

Considering the unique characteristics of roadside LiDAR, different data processing approaches have been proposed and developed recently. A common processing pipeline for roadside LiDAR data includes four major tasks: background filtering (or removal), object clustering or detection, object classification, and real-time tracking.

Background Filtering

Background filtering in a roadside LiDAR project refers to the process of separating and removing unwanted data points or noise from the main objects of interest, such as vehicles, pedestrians, and infrastructure [65]. Background points will significantly increase the computational resource and time in point cloud processing. For example, when scanning an intersection, about 30,000 points can be generated in a point cloud frame from a roadside LiDAR sensor (i.e., Velodyne VLP- 16). However, the point number of road users within the scanning range for HRMTD extraction is just about 500 points (less than 1.7% of the total points) [66]. In addition, the background filtering result will also influence the precision of HRMTD extraction. If background points are not filtered correctly and completely, the remaining background points will be identified as road users and cause misidentification of targets. In contrast, incorrect point cloud rejection can also result in

missing road users. In this regard, background filtering is crucial for improving the accuracy and efficiency of subsequent data analysis and interpretation.

Background Filtering with Static Background Construction

Static background construction is a commonly employed technique for filtering background points in point cloud processing. Zhao et al. [66] conducted a comparison between the raw LiDAR point cloud and the static background point cloud using a predefined azimuth-height table to classify points as belonging to target objects or the background. Similarly, Zhang et al. [67] determined background points by calculating the distance of each point to the static background. However, these methods necessitate manual selection of an ideal background point cloud frame, which is labor-intensive, time-consuming, and incompatible with real-time point cloud data processing and online HRMTD extraction [68].

To address this background filtering gap, Z. Zhang et al. [69] proposed a method that automatically constructs the background point cloud by utilizing the farthest and mean distance measurements for each azimuth in the LiDAR data. Y. Zhang et al. [68], on the other hand, employed a classification approach that groups subspace-frames and identifies the background group based on background characteristics. The presence of subspace frames without road users indicates the background group, with the corresponding points in that subspace designated as background points.

Alternatively, some researchers have adopted the approach of rasterizing the 3D space into isometric small cubes to construct the background. Among these methods, Wu's 3D density statistic filtering [70], [71] is widely utilized. This method involves segmenting the 3D space and overlapping frames. If the density of points within a cube exceeds a predefined threshold after overlapping, the cube is classified as background space. Additionally, some scholars have introduced a method based on changes in cube point cloud density between adjacent frames [16]. These methods exhibit high accuracy in background filtering and eliminate the need for manual frame selection. However, they require dividing the 3D space into small cubes, some as small as 0.05 m x 0.05 m per cube, to ensure accuracy, resulting in a significant increase in background construction time. Furthermore, in high-density traffic flow scenarios, achieving the desired accuracy and robustness remains challenging [68], [72].

Background Filtering Algorithms Without Static Background Construction

Several researchers have developed background filtering algorithms that do not rely on the construction of a static background. One approach is the layer-based method, which analyzes the distance distribution of LiDAR points within each layer's horizontal angles to remove background points [73]. Another method, known as channel-based filtering, utilizes channel ID information to exclude noise points from the background [74]. Additionally, a DBSCAN algorithm has been employed to filter noise based on the differences in point density and shape between ground and non-ground points. In a different study, the slice-based projection filtering (SPF) method was proposed to filter background points [21]. This method involves projecting the 3D point cloud onto

2D polar coordinates, and traffic objects are identified within an individual frame using an artificial neural network (ANN)-based model. These methods can identify objects without the need for constructing a background, resulting in improved efficiency. However, it should be noted that these algorithms or models may encounter challenges when applied to sparse point clouds, particularly in the far range of the LiDAR scanning area.

Algorithms that Improve the Detection Accuracy in the Far Range

It has been observed that the point density decreases as the distance increases [74]. This issue poses a challenge in accurately detecting road users at longer distances, where the point cloud becomes sparser. To address this issue, Zhang et al. [69] employed a projection technique on horizontal and vertical angles to construct a background dataset, thereby expanding the detection space and enhancing accuracy in further distance. Wang and Goldluecke [75] utilized the complementary properties of LiDAR, radar, and camera data to filter valid radar points as critical points, providing additional cues for the network to exploit. Moreover, some researchers have employed multiple detections to improve the detection performance of pedestrians in far-reaching areas [76]. These methods have shown promising results in the farther distant range.

While numerous innovative methods exist for background filtering in roadside LiDAR, each with its own advantages in algorithmic accuracy or operational efficiency, there remains a challenge in further enhancing the precision of background filtering algorithms. Therefore, more research is required to develop automated and highly accurate approaches for removing background points, particularly in the far detection range.

Object Detection

Object detection refers to the process of identifying and locating objects of interest, such as vehicles, pedestrians, and infrastructure, within the acquired LiDAR point cloud data [77]. This is essential for various applications, including autonomous driving, traffic monitoring, and infrastructure management [62].

It is noted that numerous LiDAR detection models are developed for self-driving applications, in which LiDAR sensors are mounted on the top of a vehicle. Recently, roadside LiDAR applications began to gain momentum as a new promising measure of traffic data collection for safety analysis and connected vehicle applications. Compared to the mobile LiDAR models that are developed for an automated vehicle to explore and understand its ever-changing surrounding environment, the roadside or stationary LiDAR is mainly to detect moving objects in a fixed setting. In a roadside LiDAR point cloud, vehicles and other road users are distributed randomly within the LiDAR scanning range. Their point features, such as density and shape, change dynamically in the space. In this case, the models that are developed based on the mobile LiDAR scanning need to be investigated for their suitability and adaptability for the detection of roadside LiDAR point clouds.

Most current object detection methods can be classified as traditional machine learning and deep learning.

Machine learning-based methods have seen significant development over the years, evolving and refining to better address object detection tasks in roadside LiDAR projects (Table 5). DBSCAN is a popular clustering algorithm that has been applied to object detection tasks in roadside LiDAR projects.

DBSCAN was introduced by Ester et al. (1996) as a density-based clustering algorithm that identifies dense regions in the data while separating noise [78]. The algorithm works by grouping points based on their density, with a user-defined distance parameter (ε) and a minimum number of points (η_min) in a neighborhood. Initially, DBSCAN was applied to generic spatial datasets. However, researchers soon recognized its potential for object detection in LiDAR data, given its ability to separate dense clusters from sparse noise points [79]. DBSCAN has been integrated with other algorithms to improve object detection performance. For example, [8] combined DBSCAN with the Hough Transform to detect and track moving vehicles in LiDAR data. A key challenge in using DBSCAN for object detection in LiDAR data is determining the optimal values for Eps and MinPts. Researchers have proposed various techniques for parameter optimization, such as using the *k*-distance graph to estimate Eps [80]. Several extensions and variations of DBSCAN have been proposed to address specific challenges in object detection tasks, including handling variable density clusters and reducing the sensitivity to parameter choices. Examples include OPTICS, which creates a hierarchical representation of the data, and HDBSCAN [81], which automatically determines the optimal number of clusters.

Machine learning-based methods have evolved over time, with various techniques and improvements being introduced to enhance object detection performance in roadside LiDAR projects. The progression from DBSCAN to ensemble methods, coupled with advancements in feature engineering and selection, has contributed to the refinement and success of these approaches.

Table 5. Summary of Machine Learning-based Methods for Object Detection

Citation	Method	Features	Classifier	Pros	Cons
[82]	SVM	Handcrafted features (e.g., geometric, statistical properties)	Support Vector Machines	Effective at finding optimal decision boundaries, good generalization performance	Requires appropriate choice of kernel function, sensitive to noise and outliers
[83]	Random Forest	Handcrafted features (e.g., geometric, statistical properties)	Random Forest	Robust to noise and overfitting, handles high-dimensional data well	Can be slow to train and predict, requires parameter tuning (e.g., number of trees)
[84]	GBM	Handcrafted features (e.g., geometric, statistical properties)	Gradient Boosting Machines	Can achieve high accuracy, handles high-dimensional data well	Requires parameter tuning, can be slow to train, sensitive to noise and outliers

SAFE-D
SAFETY THROUGH DISRUPTION

SAN DIEGO STATE UNIVERSITY   Texas A&M Transportation Institute   VIRGINIA TECH TRANSPORTATION INSTITUTE

Citation	Method	Features	Classifier	Pros	Cons
[85]	AdaBoost	Handcrafted features (e.g., geometric, statistical properties)	AdaBoost	Combines weak classifiers to create a strong classifier, can achieve high accuracy	Sensitive to noise and outliers, requires parameter tuning (e.g., number of iterations)
[80]	DBSCAN	Spatial coordinates	Density-based clustering	Automatically detects clusters of varying shapes, handles noise well	Requires appropriate choice of parameters (Eps, MinPts), not suitable for clusters with varying densities
[86]	OPTICS	Spatial coordinates	Density-based clustering	Automatically adapts to varying density clusters, does not require specifying Eps	Requires specifying MinPts, slower than DBSCAN
[81]	HDBSCAN	Spatial coordinates	Density-based clustering	Automatically determines optimal number of clusters, handles noise and varying densities well	Slower than DBSCAN, requires specifying MinPts

The emergence of deep learning-based methods has further pushed the boundaries of object detection performance thanks to their ability to automatically learn hierarchical feature representations (Table 6).

- Convolutional neural networks (CNNs)

CNNs were introduced as a method to learn local and hierarchical feature representations in image data through a series of convolutional and pooling layers (Figure 19) [87]. Researchers have adapted CNNs to process 3D LiDAR data by first converting it into a 2D image-like representation, such as a BeV or range image [88].
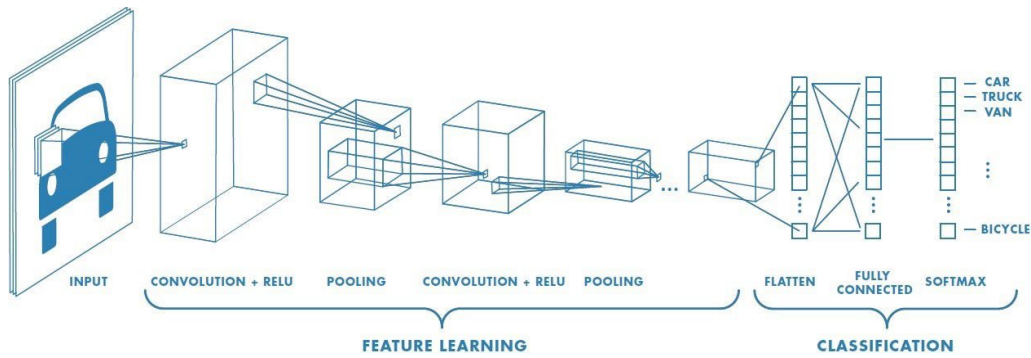
Figure 19. Diagram. Convolutional neural networks (CNNs) architecture [89].

- 3D CNNs

3D CNNs extend traditional CNNs to process 3D volumetric data directly by applying 3D convolutional and pooling operations. Researchers have utilized 3D CNNs for object detection in LiDAR data by discretizing the point cloud into voxels and feeding the volumetric representation into the network [90].

- PointNet and PointNet++

PointNet [91] was introduced as a pioneering method for processing unordered point clouds directly, eliminating the need for data conversion or voxelization. The architecture consists of a series of fully connected layers, shared Multi-Layer Perceptrons (MLPs), and a symmetric function (e.g., max pooling) to handle permutation invariance (Figure 20). PointNet++ extended PointNet by incorporating a hierarchical structure to capture local and global contextual information [91].
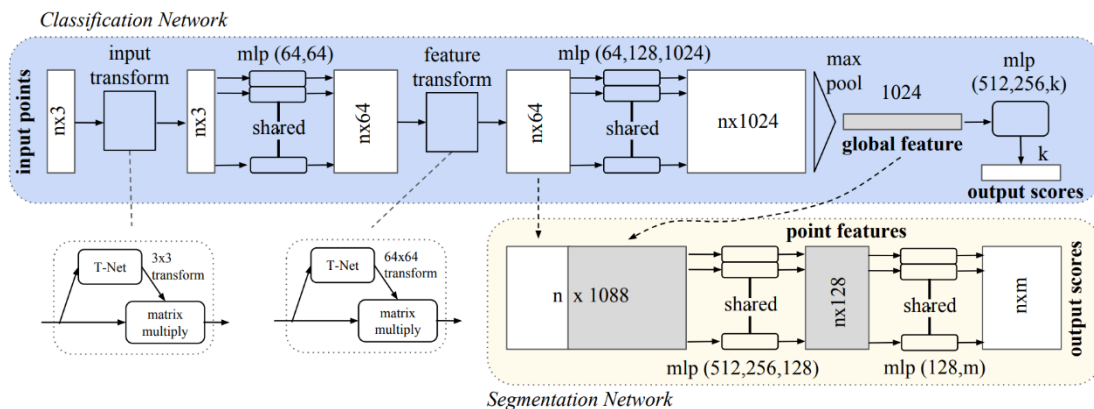

Figure 20. Diagram. PointNet architecture [92].

- Graph neural networks (GNNs)

GNNs were introduced to process irregularly structured data, such as point clouds or graphs, by modeling the relationships between nodes through graph convolutions (Figure

21). For LiDAR data, GNNs can be used to capture the relationships between points in the point cloud, enabling more effective object detection [93].
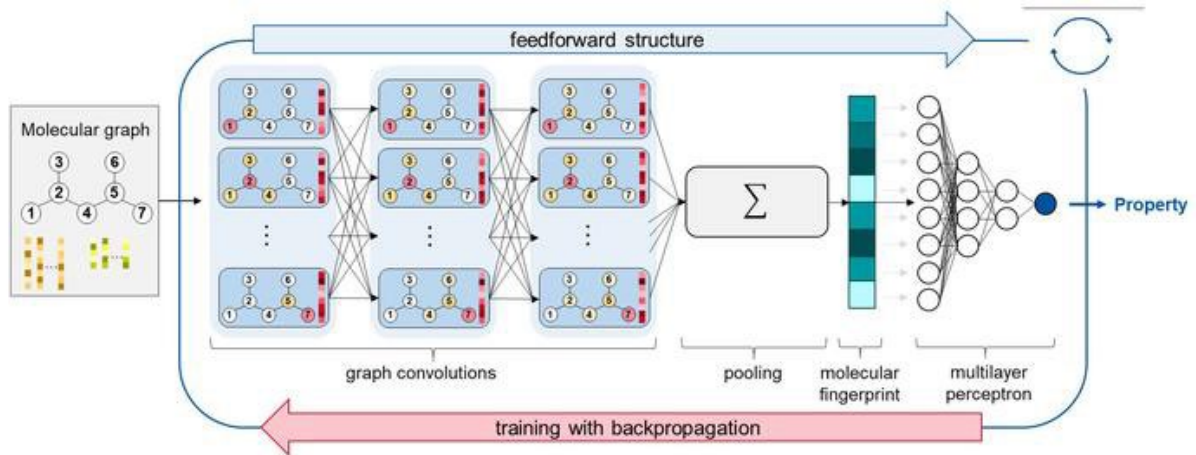

Figure 21. Diagram. Graph neural networks (GNNs) architecture [94].

- VoteNet

VoteNet is a deep learning-based method for 3D object detection in LiDAR data that uses PointNet++ as a backbone to learn point features. VoteNet utilizes a voting mechanism to generate 3D bounding box proposals by aggregating votes from points in the point cloud (Figure 22). The method is robust to varying point densities and achieves high accuracy and efficiency [91].
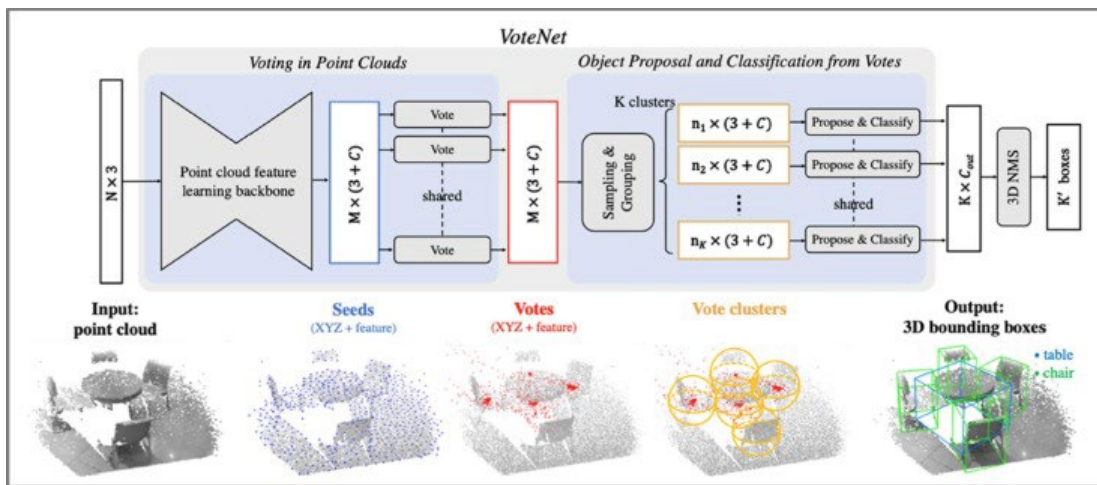

Figure 22. Diagram. VoteNet architecture [95].

- Voxel-based methods

Voxel-based methods, such as VoxelNet [96] and SECOND [97], discretize the LiDAR point cloud into a 3D voxel grid and use 3D CNNs or sparse convolutions to process the data efficiently. These methods achieve high accuracy and have been widely adopted in the autonomous driving industry.

Deep learning-based methods for object detection have evolved and been refined over time through a series of innovations, including the adaptation of CNNs to process 3D LiDAR data, the development of PointNet and PointNet++ for direct point cloud processing, the introduction of GNNs for modeling relationships in point clouds, and the development of Voxel-based methods for efficient and accurate object detection (Figure 23). These advancements have led to significant improvements in performance and paved the way for the adoption of deep learning in real-world LiDAR applications, such as roadside LiDAR object detection.
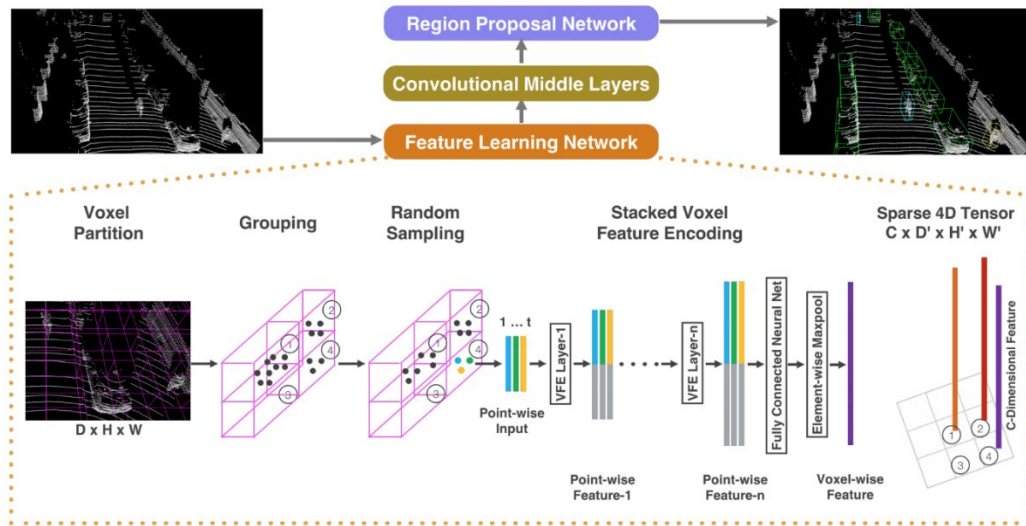

Figure 23. Diagram. VoxelNet architecture [96].

Table 6. Summary of Features of Deep Learning-based Methods for Object Detection

Citation	Method	Architecture	Data Requirement	Pros	Cons
[98]	Multi-view	2D CNNs	2D image-like representation	Utilizes existing 2D CNN architectures	Information loss during conversion
[90]	VoxNet	3D CNNs	Voxelized point cloud	Processes volumetric data directly	High computational cost and storage requirements
[91]	PointNet	Fully connected layers, shared MLPs, max pooling	Raw point cloud	Direct point cloud processing	Limited in capturing local structures
[91]	PointNet++	Hierarchical PointNet	Raw point cloud	Captures local and global contextual information	Slightly increased complexity

Citation	Method	Architecture	Data Requirement	Pros	Cons
[99]	Dynamic Graph	Graph Neural Networks (GNNs)	Raw point cloud	Models relationships in point clouds	Higher computational resources required
[96]	VoxelNet	3D CNNs	Voxelized point cloud	High accuracy and efficient processing	Loss of fine-grained details, increased memory
[97]	SECOND	Sparse convolutions	Voxelized point cloud	Efficient and accurate object detection	Loss of fine-grained details, increased memory
[100]	VoteNet	PointNet++ with voting mechanism	Raw point cloud	Robust, high accuracy, and efficient processing	Relatively complex architecture

However, the current research on object detection has several limitations:

- High computational cost: Deep learning methods, especially 3D CNNs and GNNs, can require significant computational resources for processing large-scale point cloud data.
- Loss of fine-grained details: Voxel-based methods and early approaches that convert point clouds to 2D image-like representations may result in loss of fine-grained details due to discretization or transformation.
- Sensitivity to noise and varying point densities: Some methods may be sensitive to noise or varying point densities in the point cloud data, which can affect the performance of object detection [91].
- Limited generalization capability: Machine learning and deep learning models, such as SVMs, Random Forests, or CNNs, may not generalize well across different LiDAR sensors or environments, as their performance is heavily influenced by the training data.
- Labeling and annotation challenges: Supervised learning methods require large annotated datasets, which can be expensive and time-consuming to generate for 3D LiDAR data.
- Scalability: Many methods may not scale well to handle large-scale, high-resolution, and real-time LiDAR data, which is crucial for practical applications such as autonomous driving.

Object Tracking

Object tracking and prediction involve the continuous monitoring, identification, and estimation of the future positions of objects, such as vehicles and pedestrians, within the field of view of the

LiDAR sensor. This process is crucial for various traffic monitoring and management applications and for the safety and efficiency of autonomous vehicles and advanced driver assistance systems.

Key problems that need to be addressed specifically for object tracking and prediction in roadside LiDAR projects include:

- Data association: Associating the detected objects across consecutive LiDAR frames is essential for tracking objects over time. This involves determining which object in the current frame corresponds to which object in the previous frame, considering potential issues like missed detections, false alarms, and occlusions [101].
- Object state estimation: Estimating the state (e.g., position, velocity, and orientation) of the tracked objects is a crucial aspect of object tracking. Techniques such as Kalman filtering or particle filtering can be used to estimate and update the object state based on the measurements from the LiDAR sensor [77].
- Motion modeling and prediction: Developing accurate motion models for different object types is essential for predicting their future positions and velocities. These models should account for various factors, such as road geometry, traffic rules, and typical driving behaviors [102].
- Handling occlusions and partial visibility: Roadside LiDAR sensors may not always have a complete view of the objects in the scene, leading to occlusions and partial visibility. Robust tracking algorithms should be capable of handling these situations and maintaining accurate object tracking and prediction [103].
- Real-time processing: Object tracking and prediction algorithms should be capable of processing the data in real-time to ensure timely and accurate information for traffic monitoring and management applications. This often involves optimizing the algorithms for computational efficiency and minimizing the latency [104].

For object tracking, the distance characteristics of objects between adjacent frames are commonly used in mainstream methods, such as the Hungarian method. Predictive tracking algorithms using Kalman and particle filtering are also another major type of methods [105]. Zhang et al. proposed an adjacent-frame fusion method for vehicle detection and tracking in complex traffic circumstances. In addition, the occlusion problem can be improved as well [40]. Another research study developed a tracking framework from roadside LiDAR to detect and track vehicles with the aim of accurate vehicle speed estimation [41]. Zhao et al. proposed a detection and tracking approach for pedestrians and vehicles [106]. To track the detected objects, researchers used a discrete Kalman filter to identify the same object in continuous data frames [107]. Table 7 summarizes tradition tracking methods and deep learning-based tracking methods.

Table 7. Summary of Object Tracking and Predicting Methods

Category	Method	Feature	Pros	Cons	Reference
Traditional Method	Kalman Filtering	Linear, recursive state estimation	Computationally efficient, easy to implement	Limited to linear, Gaussian systems	[108]
	Extended Kalman Filtering	Non-linear state estimation using linearization	Handles non-linear systems, computationally efficient	Inaccuracies due to linearization	[109]
	Unscented Kalman Filtering	Non-linear state estimation using deterministic sampling	Robust to non-linearities, improved accuracy	Computationally more expensive than EKF	[107]
	Particle Filtering	Non-linear, non-Gaussian state estimation using particles	Flexible, handles complex systems	Computationally intensive	[110]
	Multiple Hypothesis Tracking	Data association technique maintaining multiple hypotheses	Handles complex scenarios with interactions, occlusions	Computationally demanding	[111]
	Joint Probabilistic Data Association	Estimation of association probabilities between measurements and tracks	Handles uncertainties in data association, reduces track loss risk	Computationally intensive in high-object situations	[112]
Neural Network	Convolutional Neural Networks	Learning spatial hierarchies of features from raw data	State-of-the-art performance, handles complex data	Requires large labeled data, computationally expensive	[113]
	Recurrent Neural Networks (RNNs) and Long Short-Term Memory (LSTM) Networks	Modeling temporal dependencies in sequential data	Learns complex patterns and relationships in sequences	Requires large labeled data, computationally expensive	[114]
	Siamese Neural Networks	Learning similarity metric between image patches	Computationally efficient, suitable for real-time tracking		[115]

Category	Method	Feature	Pros	Cons	Reference
	Graph Neural Networks (GNNs)	Modeling complex relationships and interactions between objects	Handles occlusions, interactions, and long-term dependencies	Requires large labeled data, computationally expensive	[99]

There are multiple methods to evaluate the accuracy of object tracking and prediction. The commonly used evaluation metrics include:

- **Multiple Object Tracking Accuracy (MOTA):**
  MOTA is a commonly used metric that considers three error types: false positives, false negatives, and identity switches. MOTA combines these errors into a single measure, which provides a comprehensive evaluation of a tracking algorithm's performance [116].
- **Multiple Object Tracking Precision (MOTP):**
  MOTP measures the average localization error of correctly tracked objects. It provides a quantitative measure of the tracker's ability to precisely estimate object positions [116].
- **Precision and Recall:**
  Precision and recall are widely used evaluation metrics for object detection and tracking tasks. Precision measures the proportion of true positive detections among all positive detections, while recall measures the proportion of true positive detections among all ground-truth objects [117].
- **Intersection over Union (IoU):**
  IoU is a measure of the overlap between predicted bounding boxes and ground-truth bounding boxes. It is defined as the area of intersection divided by the area of union of the two bounding boxes. A higher IoU score indicates better tracking performance [117].
- **F1 Score:**
  The F1 score is the harmonic mean of precision and recall, providing a single measure that balances the trade-off between these two metrics. A higher F1 score indicates better tracking performance [118].
- **Root Mean Square Error (RMSE):**
  RMSE is a commonly used metric for evaluating the accuracy of object prediction. It measures the average squared difference between predicted and ground-truth object positions. A lower RMSE indicates better prediction performance [119].

The limitations of current research in object tracking and prediction for roadside LiDAR projects include:

- Sensitivity to noise and occlusions:

LiDAR sensors can be affected by noise, which might lead to false detections or missed objects. Additionally, occlusions caused by other objects or the environment can make it challenging to maintain accurate tracking and prediction.

- Complexity and computational demands:
  Advanced tracking and prediction algorithms, particularly those based on deep learning, often require significant computational resources and memory. This can limit their deployment in real-time or resource-constrained environments.
- Limited generalization:
  Object tracking and prediction models might not generalize well to new environments or scenarios, especially if they have not been exposed to sufficient diverse data during training. This could lead to degraded performance in real-world applications.
- Challenges in data association:
  Data association, which involves matching detected objects with existing tracks, remains a challenging problem in object tracking and prediction. Ambiguities in data association can lead to identity switches or track fragmentation, affecting overall tracking performance.

LiDAR Installation/Configuration

The major types of LiDAR sensor include (Table 8):

- Airborne LiDAR
  Airborne LiDAR systems are mounted on aircraft, such as planes or helicopters, and are commonly used for large-scale topographic mapping and environmental monitoring [120]. They can cover vast areas quickly, making them ideal for forestry, floodplain mapping, coastal zone management, and infrastructure monitoring.
- Terrestrial LiDAR
  Terrestrial LiDAR systems are ground-based and can be either stationary or mobile. They are used for detailed 3D modeling of objects, structures, and landscapes [121]. Applications include architectural documentation, structural analysis, mining, archaeology, and transportation infrastructure assessment.
- Mobile LiDAR
  Mobile LiDAR systems are mounted on moving platforms, such as vehicles or boats, allowing for rapid data acquisition in urban environments and transportation corridors [122]. Applications include road and railway infrastructure management, asset inventory, and urban planning.
- Solid-State LiDAR
  Solid-state LiDAR systems are compact and have no moving parts, making them more durable and cost-effective than traditional mechanical LiDAR sensors [123]. They are ideal for applications that require small, lightweight sensors, such as robotics, drones, and autonomous vehicles.

Table 8. Summary of Different Types of LiDAR Sensors

Classification	Feature	Application	Reference
Airborne LiDAR	Mounted on aircraft, large-scale data collection	Forestry, floodplain mapping, coastal zone management	[120]
Terrestrial LiDAR	Ground-based, stationary or mobile, high-resolution	Architectural documentation, archaeology, infrastructure	[121]
Mobile LiDAR	Mounted on moving platforms, rapid data acquisition	Road and railway management, asset inventory, urban planning	[122]
Solid-State LiDAR	Compact, no moving parts, durable, cost-effective	Robotics, drones, autonomous vehicles	[123]

Several factors can cause positional accuracy issues for LiDAR sensors:

- Occlusion: In roadside environments, objects like buildings, trees, vehicles, and other structures can obstruct the LiDAR sensor's line of sight, leading to occlusion and incomplete data collection [124].
- Multipath effects: The LiDAR sensor's laser pulses can bounce off multiple surfaces before returning to the sensor, causing false distance measurements (Figure 24). This phenomenon is common in urban environments where there are reflective surfaces, such as glass windows and metallic structures [125].
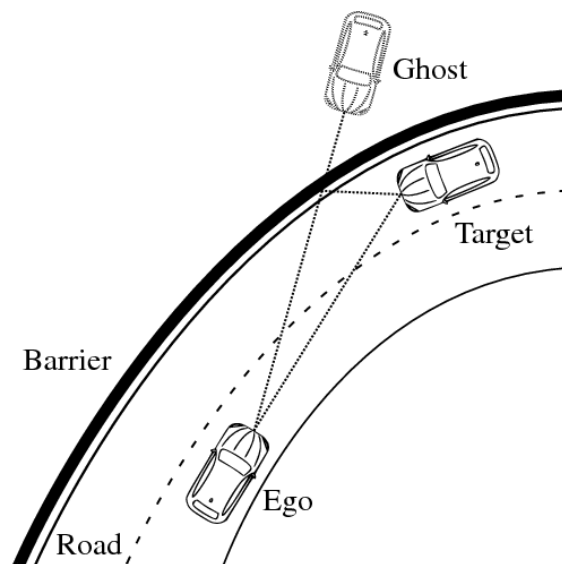

Figure 24. Illustration. Driving scenario with ghost object presence [126].

- Sensor motion: For mobile LiDAR systems, abrupt changes in speed, direction, or the sensor's angle due to road unevenness or sudden maneuvers can introduce errors in the data [122].
- Shadowing effects: When a laser pulse is obstructed by an object, a shadow is created in the scanned area behind the object. The shadowing effect can cause data gaps, making it difficult to reconstruct the complete scene [127].
- Sensor calibration: Errors in the calibration of the LiDAR sensor, including range, boresight, and mounting parameters, can result in positioning inaccuracies [128].
- Atmospheric conditions: The presence of dust, fog, rain, or snow can affect the propagation of laser pulses, causing errors in the measured distances. In addition, variations in air temperature, pressure, and humidity can impact the speed of light, leading to inaccuracies in distance measurements [129].
- GPS errors: Airborne and mobile LiDAR systems rely on GPS for georeferencing, and any errors in GPS positioning can lead to inaccuracies in the LiDAR data [130]. Factors contributing to GPS errors include satellite geometry, signal multipath, atmospheric effects, and receiver noise.
- Inertial Measurement Unit (IMU) errors: IMUs are used in combination with GPS to estimate the platform's orientation. Errors in IMU measurements, such as biases, drifts, and noise, can lead to inaccuracies in the LiDAR data (Figure 25) [131].
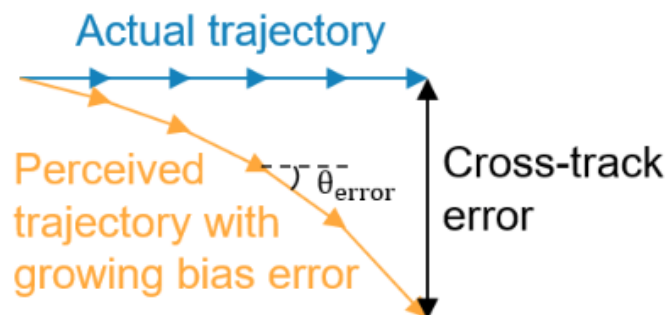

Figure 25. Graph. An example of IMU errors [132].

- Systematic errors: Errors inherent to the LiDAR sensor itself, such as range measurement errors, laser beam divergence, and scanning angle errors, can impact positioning accuracy [130].
- Target surface properties: The reflectivity, color, and texture of the target surface can influence the return signal strength and quality, affecting the accuracy of distance measurements [113].

Data Fusion for Roadside LiDAR Applications

Data fusion is the process of integrating data from multiple sources to obtain a more comprehensive and accurate understanding of a system, often resulting in improved decision-making or enhanced performance [133]. In the context of traffic data, data fusion methods are used to combine information from various traffic sensors and data sources to obtain a more complete and reliable picture of traffic conditions, travel times, and other traffic-related parameters.

The limitations of current research on data fusion for roadside LiDAR projects include:

- Heterogeneous data sources:
  Roadside LiDAR projects often involve fusing data from multiple, diverse sensors, such as cameras, radar, and LiDAR. Integrating heterogeneous data effectively remains a challenge due to differences in data formats, resolutions, and measurement errors [134].
- Scalability and computational complexity:
  Data fusion techniques can be computationally demanding, particularly when dealing with large-scale, high-dimensional, or streaming data. This can limit the real-time applicability of data fusion methods in roadside LiDAR projects [135].
- Sensor noise and uncertainty:
  Sensor noise and uncertainty can adversely affect data fusion performance. Developing robust methods to handle sensor noise and model uncertainties is a key challenge in data fusion research for roadside LiDAR projects [134].
- Synchronization and alignment:
  Temporal synchronization and spatial alignment of data from multiple sensors is crucial for accurate data fusion. Achieving precise synchronization and alignment can be challenging, particularly when dealing with large-scale, dynamic environments [136].
- Lack of standardized evaluation methods:
  There is a lack of standardized evaluation methods and benchmarks for assessing the performance of data fusion techniques in roadside LiDAR projects. This makes it difficult to compare different approaches and gauge their real-world applicability [134].

Appendix B: More Information for Data Collection

Simulated Datasets

This project aimed to develop and implement a set of algorithms for a roadside LiDAR-based work zone intrusion system. The system can conduct vehicle trajectory analysis and threat assessment needed to accurately provide advanced warning to workers for any possible vehicle intrusion in the work zone. However, researchers found that recreating these intrusion scenarios and the needed traffic environment in the real world requires significant time, resources, and expense, and may present high risks in tests. Therefore, simulation of the system seems like a particularly safer and more efficient option before we implement it in the field.

The main purpose of the simulation study was to use a 3D virtual environment to enable testing of roadside LiDAR applications, which will significantly reduce the amount of required road tests in the real world. The simulation was based on a co-simulation framework for modeling and visualizing driving algorithms in MATLAB Simulink® in a rich simulation environment powered by Unreal Engine®. The testing results facilitated the development of perception and control algorithms, verified the system's functionality, and improved robustness at the system level. The developed simulation framework also demonstrated that it can run at sufficient frame rates for real-time computations on a reasonable desktop workstation leveraging the power of a graphics processing unit (GPU). The major contributions of this simulation work are the following:

- Development of a co-simulation framework for roadside LiDAR applications by using MATLAB, Simulink, and Unreal Engine.
- Demonstration of the developed simulation framework in a SWZ case study to show its capacity for assisting the system development and its adaptability to other roadside LiDAR applications.

Simulation

In the simulation, researchers used MATLAB as the basic simulation software development platform to verify the rationality of the design parameters of the roadside LiDAR-based system. The simulation results showed that the software platform consistently and robustly achieved the purpose of evaluating and guiding the design process of system parameters.

MATLAB provides a co-simulation framework for modeling and visualizing driving algorithms in Simulink in a rich simulation environment powered by the Unreal Engine from Epic Games (Figure 26). With this simulation environment, researchers can configure prebuilt scenes, place and move vehicles within the scene, and set up and simulate sensors (i.e., camera, radar, or LiDAR) on the vehicles or at the roadside. A photorealistic 3D environment and sensor detections of objects can be simulated and outputted for analysis by generating simulated driving scenarios.
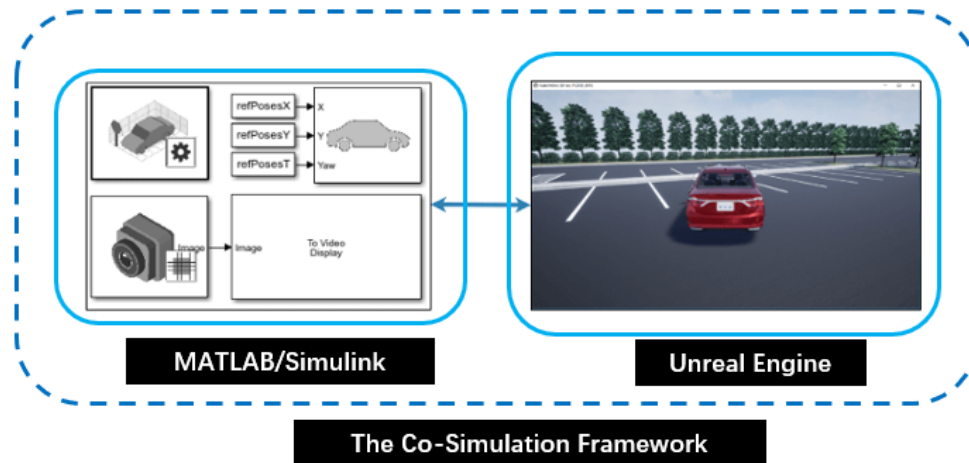
Figure 26. Diagram. The co-simulation framework that is built on MATLAB/Simulink and Unreal Engine [22].

Simulation Procedures

In the simulation, Unreal Engine creates 3D virtual driving environments and dynamic scenarios, supports the exporting of data to MATLAB over shared memory, and acquires data about the 3D environment necessary to generate synthetic sensor data (i.e., camera and LiDAR data). Environments created in this method can achieve a realistic, detailed appearance and geometry for the generation of synthetic camera and LiDAR data. Meanwhile, MATLAB and Simulink can process this data and develop prototype perception and control algorithms. This includes toolboxes for computer vision, image processing, and LiDAR point cloud processing, which is integrated in MATLAB Automated Driving Toolbox [137]. Therefore, an interface is enabled between MATLAB/Simulink and Unreal Engine, which allows a full pipeline to be tested that includes these capabilities. The following diagram in Figure 27 summarizes the communication between MATLAB/Simulink and the visualization engine (Unreal Engine).
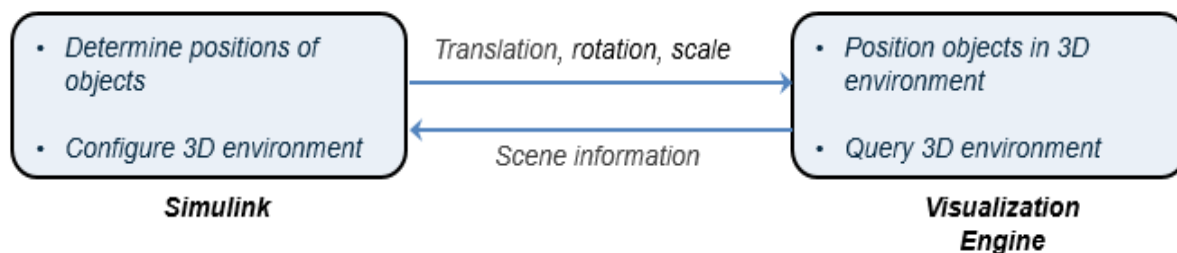

Figure 27. Diagram. Communication flows between MATLAB/Simulink and Unreal Engine [22].

Simulink Blocks

Simulink blocks related to the simulation environment can be found in the automated driving toolbox in MATLAB. These blocks provide the ability to: 1) configure scenes in the simulation environment; 2) place and move vehicles within these scenes; 3) set up camera, radar, and LiDAR sensors on the vehicles; 4) simulate sensor outputs based on the environment around the vehicle;

and 5) obtain ground truth data for semantic segmentation and depth information. Figure 28 shows the Simulink blocks created for the SWZ case study.
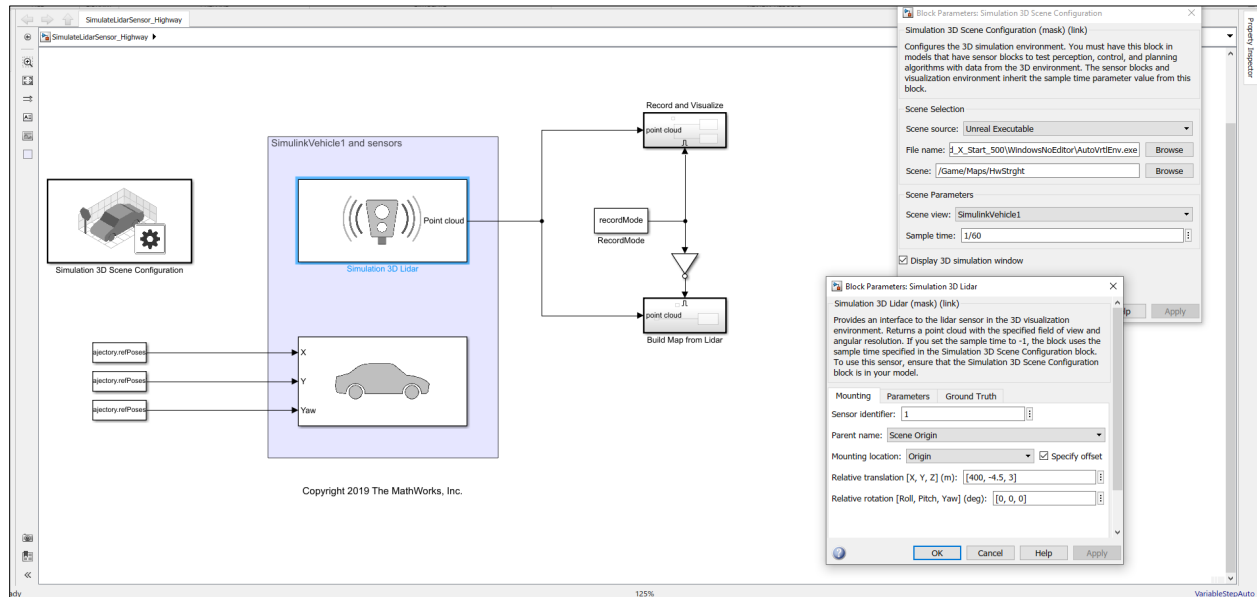

Figure 28. Screen shot. MATLAB/Simulink blocks in a designed simulation model for the SWZ case study [22].

Unreal Engine Blocks

During the simulation, Unreal Engine executes its simulation blocks in a specific order. First, the simulation 3D Vehicle with Ground Following blocks initialize the vehicles and send their **X, Y,** and **Yaw** signal data to the Simulation 3D Scene Configuration block. Next, the Simulation 3D Scene Configuration block sends the data to the sensor blocks. Finally, the sensor blocks use the data to accurately locate and visualize the vehicles. The **priority** property of the blocks controls this execution order (as shown in Figure 29). By default, Simulation 3D Vehicle with Ground Following blocks have a priority of -1, Simulation 3D Scene Configuration blocks have a priority of 0, and sensor blocks have a priority of 1.
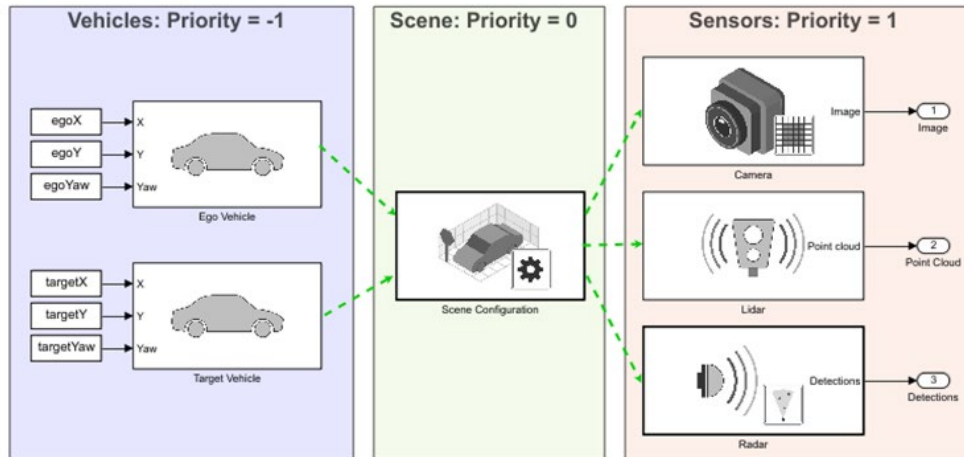
Figure 29. Diagram. Execution order for Unreal Engine simulation blocks [22].

In conjunction with vehicle models and driving algorithms, these blocks can be used to perform realistic closed-loop simulations that encompass the entire automated driving stack, from perception to control. Figure 30 shows a roadside LiDAR-based SWZ application with LiDAR output results. The LiDAR sensor was placed at the beginning of the work zone transition area (as delineated by traffic cones).
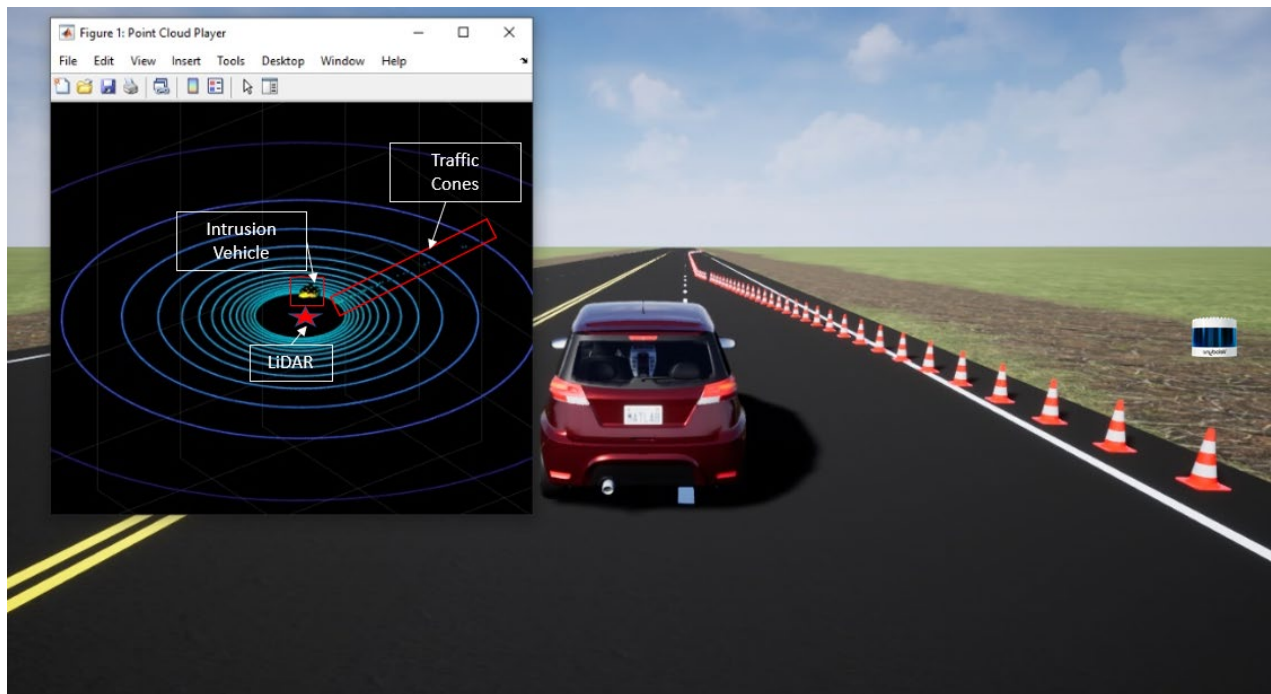

Figure 30. Illustration and screen shot. Visualization of a SWZ application with LiDAR output in Unreal Engine [22].

Data Collection from Test Sites

Two datasets, which will be publicly available for other researchers,[3] were collected with a Velodyne VLP-16 sensor, mounted at 2.2 meters high on a portable tripod in two different sites (Table 9). The first dataset, named 01-TAMU, was collected on a six-lane urban road segment, though the primary ROIs covers one travel direction (three lanes). The second dataset (Figure 31), named 02-TAMU, was collected on a four-lane highway segment, with again the primary ROI covering one travel direction (two lanes). Quantitative analysis of 01-TAMU and 02-TAMU was made available through hand-annotated LiDAR data of several hundred frames with vehicles in-scene.

This dataset contains two approximately 10-minute segments on an urban (45 mph) and highway segment (75 mph), consisting of >1,000 frames labeled of measurements taken with a Velodyne VLP-16. The dataset format is as follows:

- Raw (unprocessed ROI filtering) data in rosbag data format[4]
- BeV projection images of LiDAR data
- Labels in .csv format for each image

Table 9 summarizes the dataset:

Table 9. Description of 01-TAMU and 02-TAMU Datasets

Dataset	Description	Total Duration mm:ss	# Annotated Frames	Total Annotated Vehicles	ROI (m)
01-TAMU	45 mph / 72 kph 6-lane urban road coords: 30° 37'16.6"N 96° 20'30.7"W	09:51	546	41	$X: -1, 15.5$ $Y: -30, 30$ $Z: -1, 3$
02-TAMU	75 mph / 120 kph 4-lane highway coords: 30° 38'55.5"N 96° 28'35.4"W	09:43	549	13	$X: -1, 21$ $Y: -40, 40$ $Z: -3, 3$

---

[3] The dataset will be available through the SAFE-D Data Portal

[4] Rosbag format data refers to recorded bags of messages in the Robot Operating System (ROS), which are commonly used for storing and replaying robotic system data
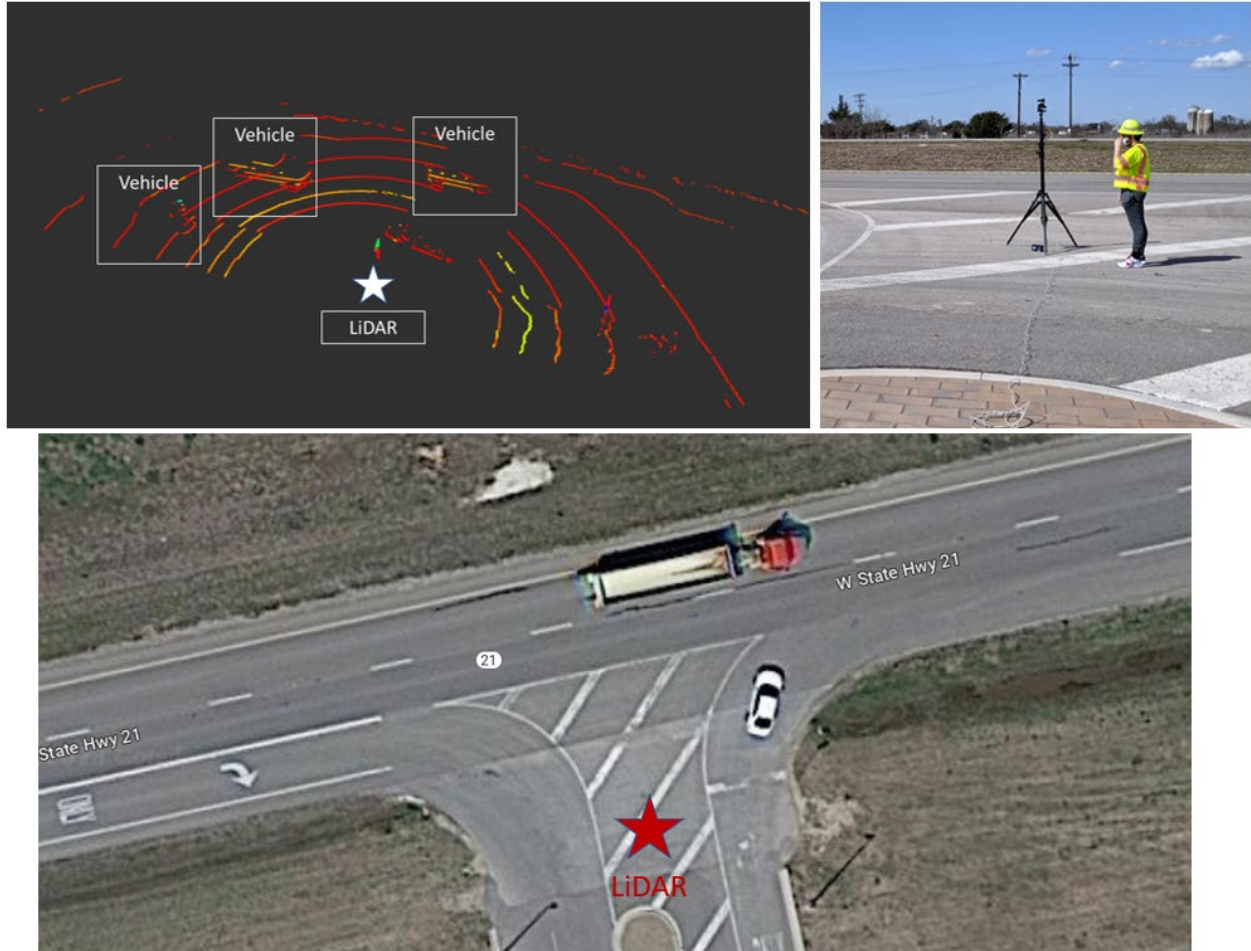
Figure 31. Graph and photos. The data collection site on the RELLIS Campus (02-TAMU).

Experimental Work Zone Data Collection

Purpose

The data from this experimental work zone collection was to test and validate the developed detection and tracking algorithms through some designed scenarios under a controlled testing environment on the TAMU RELLIS Campus. The test aimed to measure/quantify the system's reliability, accuracy, and computation efficiency. Through the experiment, researchers also investigated the optimal LiDAR detection system setup for given specific work zone configurations (e.g., single vs. multiple sensors, location, height and alignment of the sensors) and vehicle intrusion scenes (e.g., high speed or low speed intrusions, different intrusion types). The test data were used to improve the algorithms and prepare the team for the implementation in a real work zone environment.

The research facilities on the RELLIS Campus allow faculty, students, and private-sector partners to collaborate on cutting-edge research and technology development activities while benefiting from the use of the proving grounds and testbeds that will be available at the RELLIS Campus.

These testbeds and proving grounds afford large-scale testing of the technologies developed through these collaborations in a safe and controlled environment.

The proving grounds of the facility have multiple runways, aprons, and transportation-related pavements, signs, and markings, which make them ideal research testing sites (Figure 33). The proving ground (or runaway) area reserved for this field experiment is highlighted in yellow in Figure 32: 35L Sect 1, 35L Sect 2, 35L Sect 3, 35L Sect 4, Taxi 7 Sect 5. The area has two painted lanes on the west side of runaway.

Figure 32. Satellite image. The TAMU RELLIS Campus testing facility.

Figure 33. Satellite image and photo. The experimental work zone data collection site in the RELLIS Campus.

Experimental Work Zone Tests

In the experimental data collection, the team collected the data under several controlled work zone settings and vehicle intrusion scenarios. There are many possible work zone configurations in the real world. However, due to time and resource limits, this proof-of-concept study only investigated a specific work zone configuration based on the literature review and expert suggestions: a single lane closure on a four-lane highway segment (two-lane in each direction). Researchers designed two tests for this specific work zone configuration:

- Test 1: One lane closure on a high-speed four-lane highway (60 mph)
  - Single LiDAR sensor settings
  - Multiple LiDAR sensor settings (two LiDAR sensors)
- Test 2: One lane closure on a low-speed four-lane road (30 mph)
  - Single LiDAR sensor settings
  - Multiple LiDAR sensor settings (two LiDAR sensors)

Various LiDAR setup factors were also considered in the experiments, including but not limited to: mounting or installation method, height and location of LiDAR sensor(s) in the work zone, detecting range, alignment of multiple sensors (if needed), etc. The optimal configuration for LiDAR sensor(s) was determined for this specific work zone configuration by the testing results and the theoretical analysis. Temporary traffic cones or barriers were placed to indicate work zone areas for the target vehicles. No other installation was required.

Test 1: One Lane Closure on a High-speed Two-lane Highway (60 mph Speed Limit)

In this test, the team designed a one-lane closure scenario on a high-speed two-lane highway segment. The highway has a standard lane width of 12 ft and shoulder width of 10 ft. However, the shoulder on 35L has a width of 12 ft, which allowed additional room in the experimental testing. The posted speed limit for the highway is set as 60 miles per hour.

Figure 34 shows the designed work zone configurations. In this case, the transition area (or the buffer area) of the work zone should be at least 720 ft long according to the Manual on Uniform Traffic Control Devices (MUTCD); 250 ft is advanced signing before transition area.
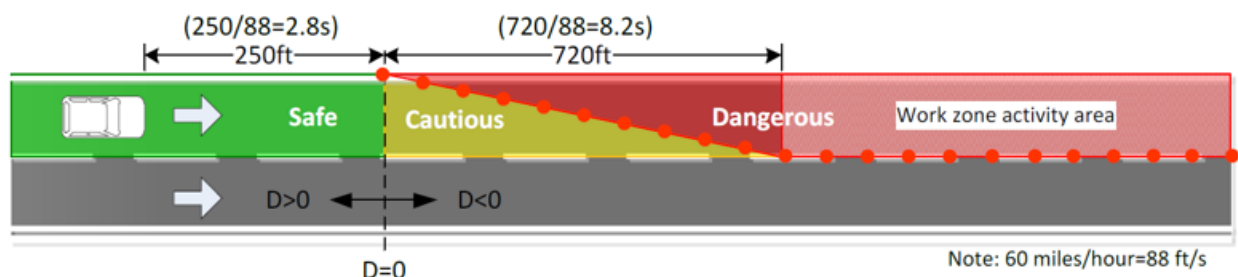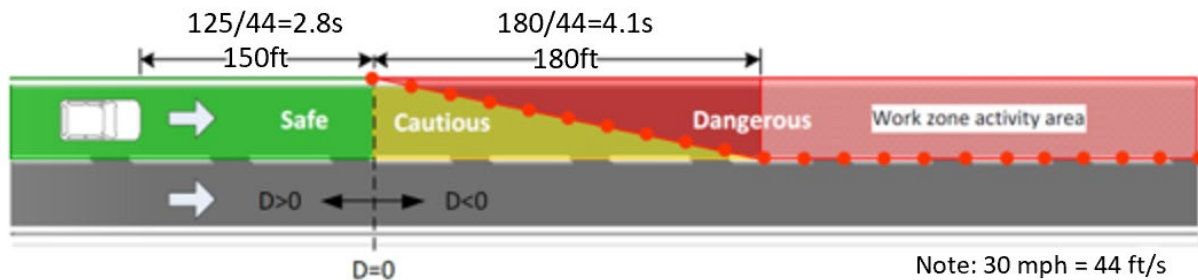

Figure 34. Diagram. High-speed two-lane highway work zone configurations [19]. (D is the distance to start of the taper).

Test 2: One Lane Closure on a Two-lane Road with Two LiDAR Sensors (30 mph Speed Limit)

In this test, the team designed a one-lane closure scenario on a low-speed road segment (the posted speed limit is 30 mph), which was intended to represent a construction work zone on a local street.

Figure 35 shows the designed work zone configurations. In this case, the transition area (or the buffer area) of the work zone should be at least 180 ft long.

Figure 35. Diagram. Low-speed two-lane highway work zone configurations.

LiDAR Configuration

The LiDAR configuration was changed depending on whether one or two sensors were operated at a time. There are three parameters of interest for this study: the longitudinal placement along the travel direction, the lateral placement across the lane, and the mounting height. The LiDAR's roll, pitch, and yaw angles were fixed to 0 degrees.

When testing a single LiDAR, the placement was closest to the intrusion area, labeled with a numeral 1 in the two scenarios below. When testing two LiDARs, an additional LiDAR (labeled 2) was added to the work zone with overlapping coverage from the first LiDAR. The separation distance should not exceed 30 m between two LiDARs to maintain overlapping coverage.

Table 10. LiDAR Configuration Parameters

Parameter	Testing Range	Unit
D_v (vertical mounting distance)	1.6-2.5	Meter
D_h (horizontal setback distance)	1.0-8.0	Meter
Δ_x (longitudinal separation distance)	15.0-30.0	Meter

Vehicle Intrusion Scenarios

Two work zone collision types have been investigated in the test. Since these are experiments, the actual work zone cones should not be placed. Instead, the cones were used to create channeling guides for the test vehicles to maneuver safely into the work zone.

Testing Scenario 1: Buffer Zone Collision

The buffer zone collision test collected data from a simulated full-frontal collision from the buffer zone as shown in Figure 36 and Figure 37. This test was planned to be conducted at 30 and 60 mph. A minimum stopping distance of 1,000 ft allowed the vehicle to safely slow after the

maneuver was complete. The width of the lane for travel was at a minimum 12 ft. No testing personnel were in the work zone area due to safety concerns.
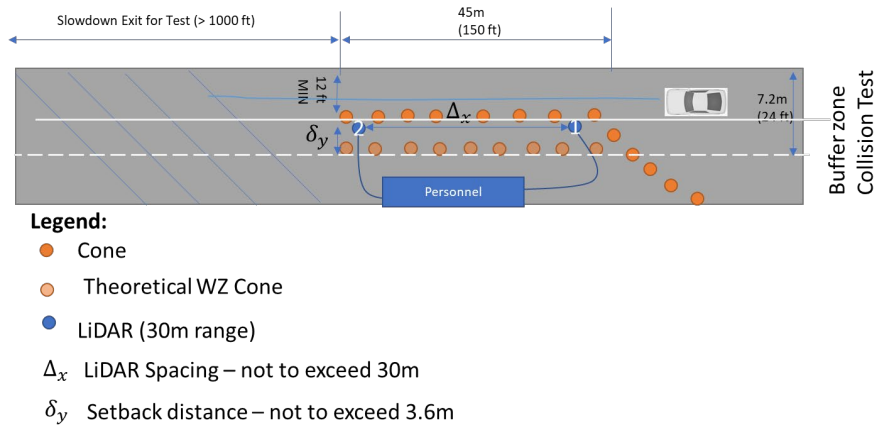

Legend:
- ● Cone
- ◉ Theoretical WZ Cone
- ● LiDAR (30m range)
- Δ_x LiDAR Spacing – not to exceed 30m
- δ_y Setback distance – not to exceed 3.6m

Figure 36. Diagram. Settings of Testing Scenario 1.
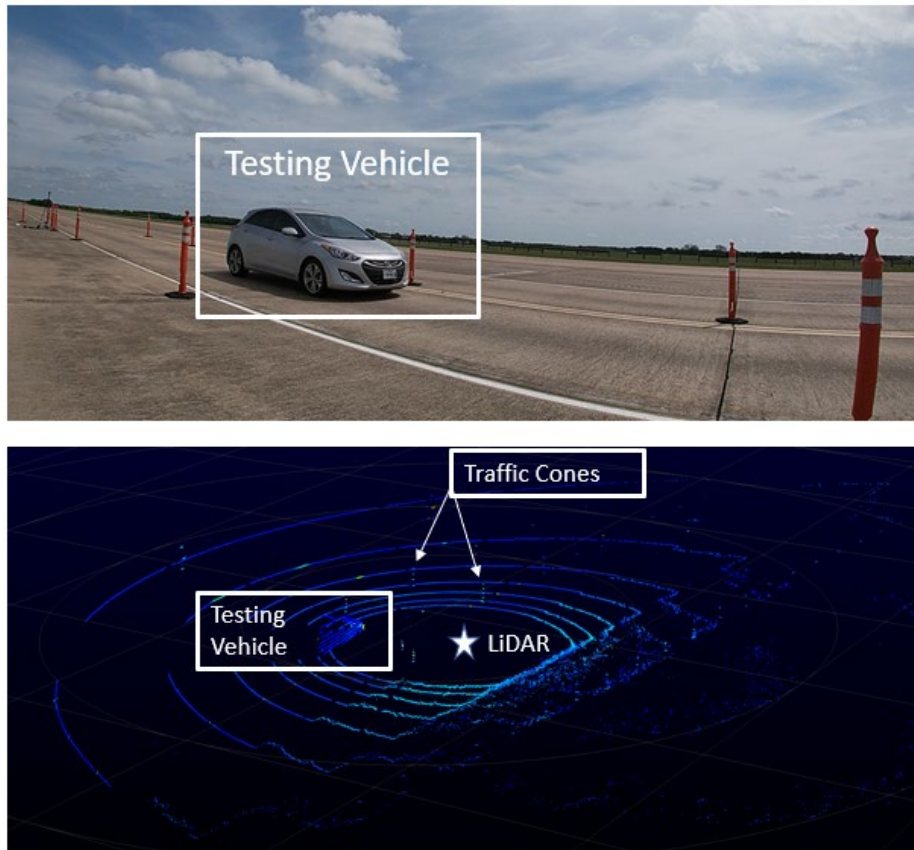
Figure 37. Photo and graph. Visualization of Scenario 1's LiDAR outputs.

Testing Scenario 2: Side Sweep Collision

The second scenario to be tested was the side sweep collision scenario (Figure 38, Figure 39). For safety, this scenario was conducted at only 30 mph. Personnel were behind or in front of the work

zone collision, depending on the number of LiDARs used. Cones were used to channel the vehicle safely into the work zone, emulating a gradual intrusion crash. A minimum stopping distance of 1000 ft allowed the vehicle to safely slow after the maneuver was complete. The width of the lane for travel should be at a minimum 12 ft.
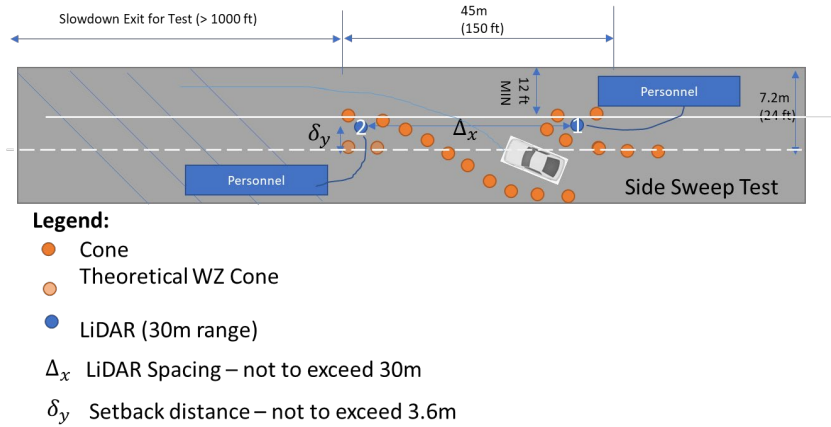

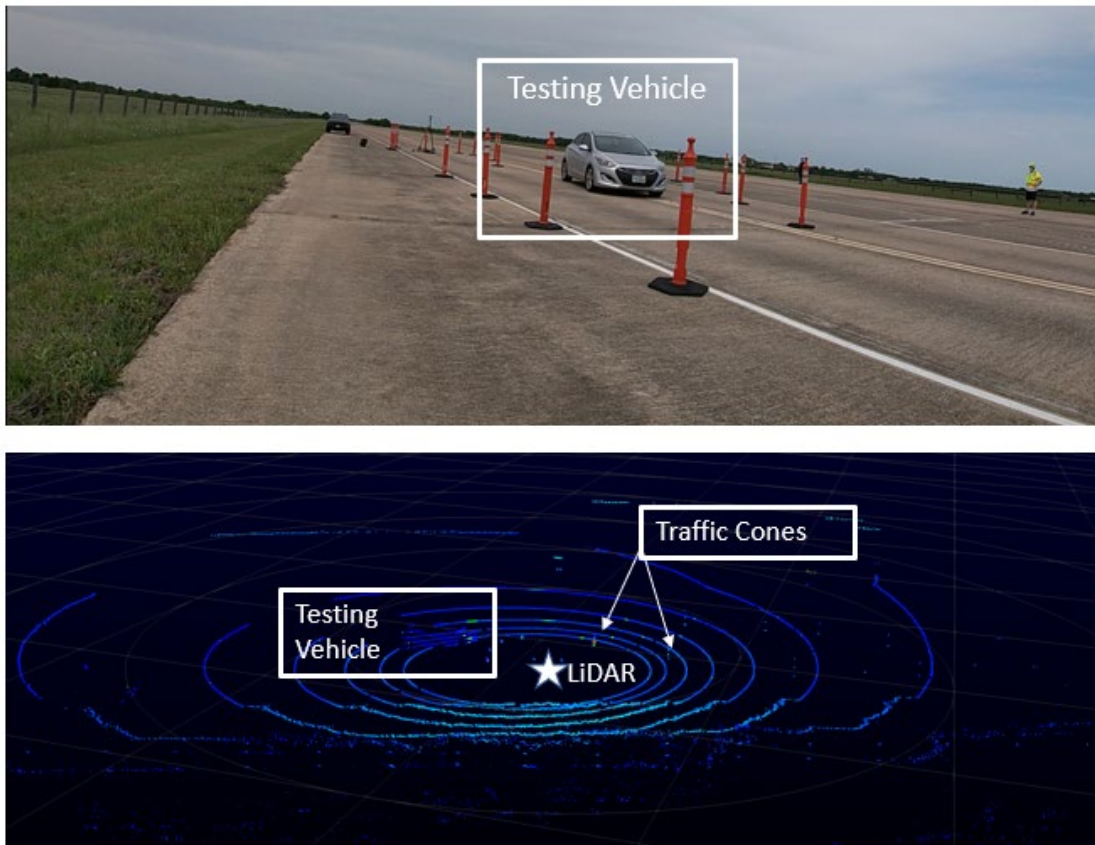**Figure 38. Diagram. Settings of Testing Scenario 2.**

Figure 39. Photo and graph. Visualization of Scenario 2's LiDAR outputs.

In this scenario, the testing team used LiDARs to collect simulated workers' activities by having personnel walk around in the work zone area (Figure 40).
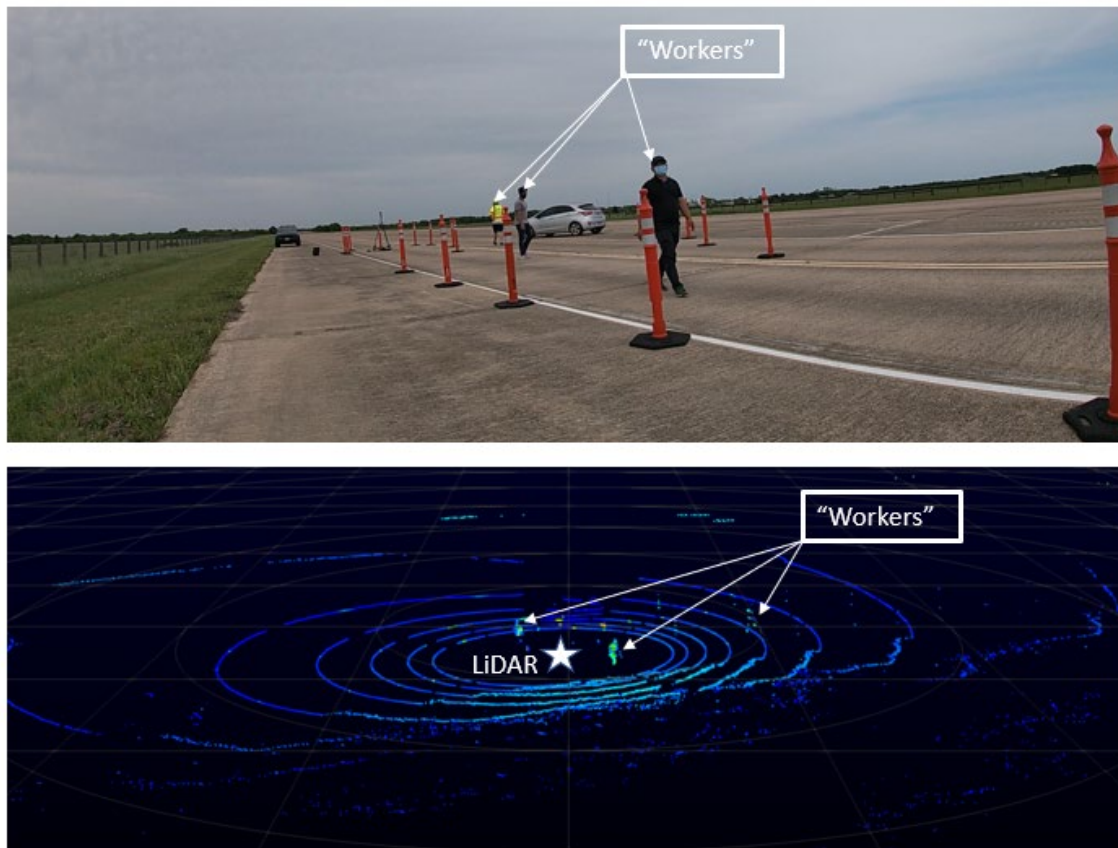

Figure 40. Photo and graph. Visualization of Scenario 3's LiDAR outputs.

Real Work Zone Data Collection

The research team continued to collect data from a real work zone environment. Researchers worked closely with the Texas DOT (TxDOT) Dallas District to identify work zone sites appropriate for the purpose of this project. Two sites were located on US-380, as shown in Figure 41. US-380 is a major highway located in the areas of Denton and Collin counties in Texas. It serves as a critical transportation route, connecting various cities and communities within the region. The highway plays a pivotal role in facilitating transportation and supporting economic activities in the region. With its proximity to populated areas and diverse traffic conditions, US-380 offers a suitable environment for conducting research, testing, and implementing innovative technologies and safety measures aimed at enhancing the efficiency and safety of the roadway system.

These sites represented typical cross-sections of the highway and work zone elements, including traffic lanes, shoulders, median, signage, and temporary barriers (Figure 42). The posted speed

limit at the sites (50 mph[5]) was recorded to establish a baseline for system performance. LiDAR technology was utilized as the primary sensor system, generating detailed 3D point clouds to detect and track vehicles and potential intrusions within the work zone. The collected data will contribute to refining intrusion detection algorithms and enhancing work zone safety measures on US-380 (note that this may not be within the scope of this project).

Figure 41. Satellite image. The identified TxDOT work zone sites.

---

[5] Due to safety concerns, the speed limit on US-380 at the locations designated for data collection, where a construction widening project is currently in progress, is being decreased to 50 mph.

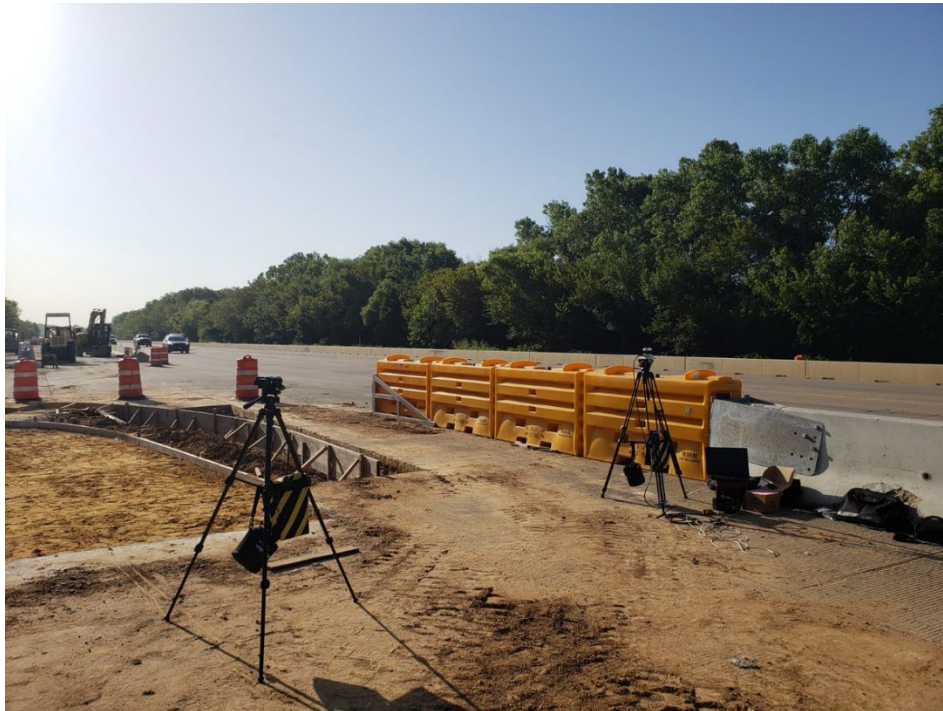**Figure 42. Photo. Site photo of the identified work zone sites on US-380.**

Figure 43. Photo. The LiDAR setup in the work zone.